2009

SST, thermohaline structure, and circulation in the southern Gulf of California in June 2004 during the North American Monsoon Experiment

Lavín, M.F.

SST, thermohaline structure, and circulation in the southern Gulf of California in June 2004

SST, thermohaline structure, and circulation in the southern Gulf of California in June 2004 during the North American Monsoon Experiment

M. F. Lavín,[1] Rubén Castro,[2] Emilio Beier,[3] Victor M. Godínez,[1,2] Alberto Amador,[1] and P. Guest[4]

Received 30 April 2008; revised 15 October 2008; accepted 22 December 2008; published 28 February 2009.

[1] The thermohaline structure, circulation, and heat fluxes in the Gulf of California entrance during June 2004 are described based on conductivity-temperature-depth and Lowering Acoustic Doppler Current Profiler data collected in a 14-day survey, supported by satellite data. The AVHRR images show extensive mesoscale structures in the region, the most striking being (1) a cool filament extending from the California Current domain and (2) a warm intrusion along the mainland shelf. On the warm side of the thermal front created by the cool filament there was a strong current flowing into the Gulf, with speeds up to 0.70 ms^{-1} in the surface; this current, which the SST images suggest was associated with a decaying eddy, carried 6 Sv into the Gulf. Associated with the second structure, there was an ingoing coastal current on the mainland shelf, with weak surface currents but with speeds $\sim$0.25 ms^{-1} at its core, between 70 and 200 m; this coastal current transported 2 Sv into the Gulf. The two ingoing currents appear to join inside the Gulf, forming a very strong (speeds 0.40–0.80 ms^{-1}) narrow ($\sim$30 km) coastal current between the surface and 500 m depth. Changes in the thermohaline structure of the upper layers observed by repeat sampling of three cross sections were dominated by advection. However, it was found that the advective heat flux is very variable in space and time. For the period of observation it was estimated that the lateral heat input was $4.8 \pm 3.0 \times 10^5$ Wm^{-2} as estimated with LADCP currents and $5.7 \pm 2.20 \times 10^5$ Wm^{-2} with geostrophic velocities.

Citation: Lavín, M. F., R. Castro, E. Beier, V. M. Godínez, A. Amador, and P. Guest (2009), SST, thermohaline structure, and circulation in the southern Gulf of California in June 2004 during the North American Monsoon Experiment, *J. Geophys. Res.*, *114*, C02025, doi:10.1029/2008JC004896.

1. Introduction

[2] The summer 2004 North American Monsoon Experiment (NAME), part of NOAA's PACS/GAPP Warm Season Precipitation Initiative, was an intensive observational study of the meteorological fields in and around the Gulf of California (GC). Many of the meteorological studies have been published in a special issue of *Journal of Climate* [*Higgins and Gochis*, 2007]. Although generally accepted that the GC is important to the North American Monsoon (NAM) and therefore for the precipitation in NW Mexico, Arizona, and New Mexico, there are questions as to what role it actually plays, in addition to channeling the low-level moisture flux [*Higgins et al.*, 1999]. The sea surface temperature (SST) in the GC is a potentially important parameter in determining the onset and intensity of the NAM [*Mitchell et al.*, 2002], yet we only have a limited understanding of what mechanisms control its evolution.

[3] The communication of the Gulf of California (Figure 1) with the Pacific Ocean is $\sim$3000 m deep and $\sim$200 km wide. The seasonal balances of heat and salinity are not controlled by the surface heat and moisture fluxes but by the interaction with the Pacific, and although there are no studies focusing on how the SST and the sea surface salinity are controlled, there is evidence that advection has an important role [*Castro et al.*, 1994; *Ripa*, 1997; *Beron-Vera and Ripa*, 2000, 2002; *Zuidema et al.*, 2007]. The climatological monthly progression of the SST in the GC and in the neighboring Pacific, based on AVHRR data, is shown in Figure 2. The fastest seasonal surface heating inside the GC occurs from May to July, with the isotherms turning north-south in May and along-gulf in June and July. The across-gulf SST gradient during summer has been interpreted [*Soto-Mardones et al.*, 1999] as evidence of upwelling induced by the summer SE winds, but *Mitchell et al.* [2002] suggested that the May–July SST evolution described above could be due to the advection of warm water from the southeast.

[4] The surface atmospheric circulation in the GC differs markedly from that in the Pacific adjacent to the peninsula

[1]Departamento de Oceanografía Física, CICESE, Ensenada, Mexico.
[2]Facultad de Ciencias Marinas, Universidad Autónoma de Baja California, Ensenada, Mexico.
[3]Estación La Paz, CICESE, La Paz, Mexico.
[4]Naval Postgraduate School, Monterey, California, USA.

0148-0227/09/2008JC004896

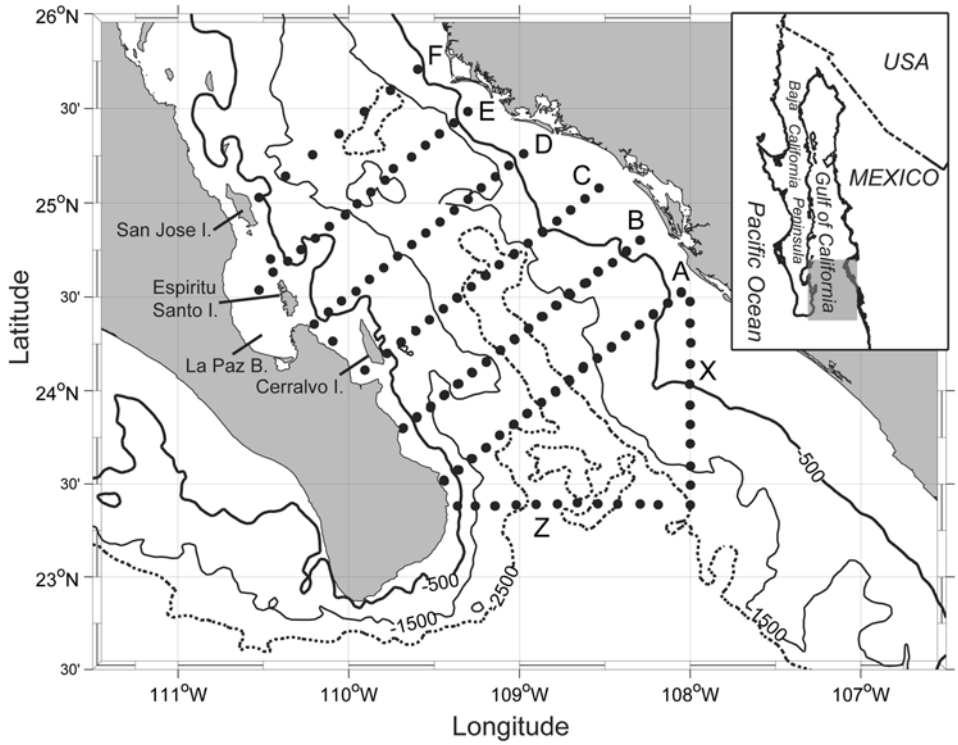

Figure 1. Study area, with bathymetry (depth is in meters). The black dots show the position of the oceanographic stations. The sections of stations are identified by the letters Z, X, and A to F (in order of sampling). Sections A, B, and C were repeated after section F.

of Baja California; while in the Pacific the wind has a strong NW component almost year-round which intensifies in spring and part of summer [*Strub and James*, 2002], in the GC the NW winds dominate most of the year, but they turn to SE in late spring and summer [*Bordoni et al.*, 2004].

[5] The thermohaline structure of the upper layers in the area where the communication with the Pacific takes place, which will be called "the entrance," is very complex due to the confluence of surface waters with very dissimilar characteristics [*Griffiths*, 1968; *Álvarez-Sánchez et al.*, 1978; *Castro et al.*, 2000; *Lavín and Marinone*, 2003]: Tropical Surface Water (TSW), California Current Water (CCW) of subarctic origin, and the Gulf of California Water (GCW). The temperature and density differences between these surface water masses cause sharp fronts, which tend to develop mesoscale structures like eddies, jets, and meanders, which are ubiquitous in the area, as can be seen in the AVHRR images in Figure 3. In the vertical, interleaving, uplifting, and submergence can also be produced, with the denser CCW and GCW tending to be found underneath the TSW [*Castro et al.*, 2000]. Although there is a generally accepted classification of these surface water masses according to their temperature and salinity (Table 1; also see review by *Lavín and Marinone* [2003]), we will see that care should be exercised when using it to classify a given water volume in this area.

[6] Immediately below the surface water masses, starting at ~150 m depth, there is the Subtropical Subsurface Water (StSsW), characterized by a salinity maximum (~34.7–34.8, Table 1) at a depth of ~150–200 m; we will retain this water mass name although it is now considered to be modified 13°C Water [*Fiedler and Talley*, 2006] brought from the equatorial zone to the eastern tropical Pacific by the Northern Tsuchiya Jet. There can be much interaction between the StSsW and the surface water masses described above, again making water mass classification somewhat ambiguous. The two remaining deeper water masses, the Pacific Intermediate Water and the Pacific Deep Water are stable at the seasonal timescale.

[7] *Castro et al.* [2000] constructed a mean and a seasonal description of the thermohaline structure in a single cross section in the entrance to the GC (close to section A of Figure 1), based on eight crossings made between 1992 and 1998. In the mean, they find that in the upper 200 m the thermohaline field shows warm and relatively fresh water over the mainland shelf (CCW and TSW), and relatively less warm and saltier water close to the peninsula (GCW). *Mascarenhas et al.* [2004] used the same data set to obtain a mean and a seasonal description of the geostrophic currents at the entrance cross section. They found that in the mean there is ingoing flow on the mainland side and outgoing flow on the peninsula side, which is in agreement with previous descriptions based on less data [*Roden*, 1964, 1971; *Warsh and Warsh*, 1971; *Collins et al.*, 1997]. However, their data also revealed very large spatial variability, with alternating in-going and out-going jets. Since their data and other high-density samplings in the same area showing similar variability are based on single cross sections [*Roden*, 1972; *Collins et al.*, 1997], the doubt arises as to whether those features represent steady currents or reflect mesoscale activity, such as the eddies and meanders in Figure 3.

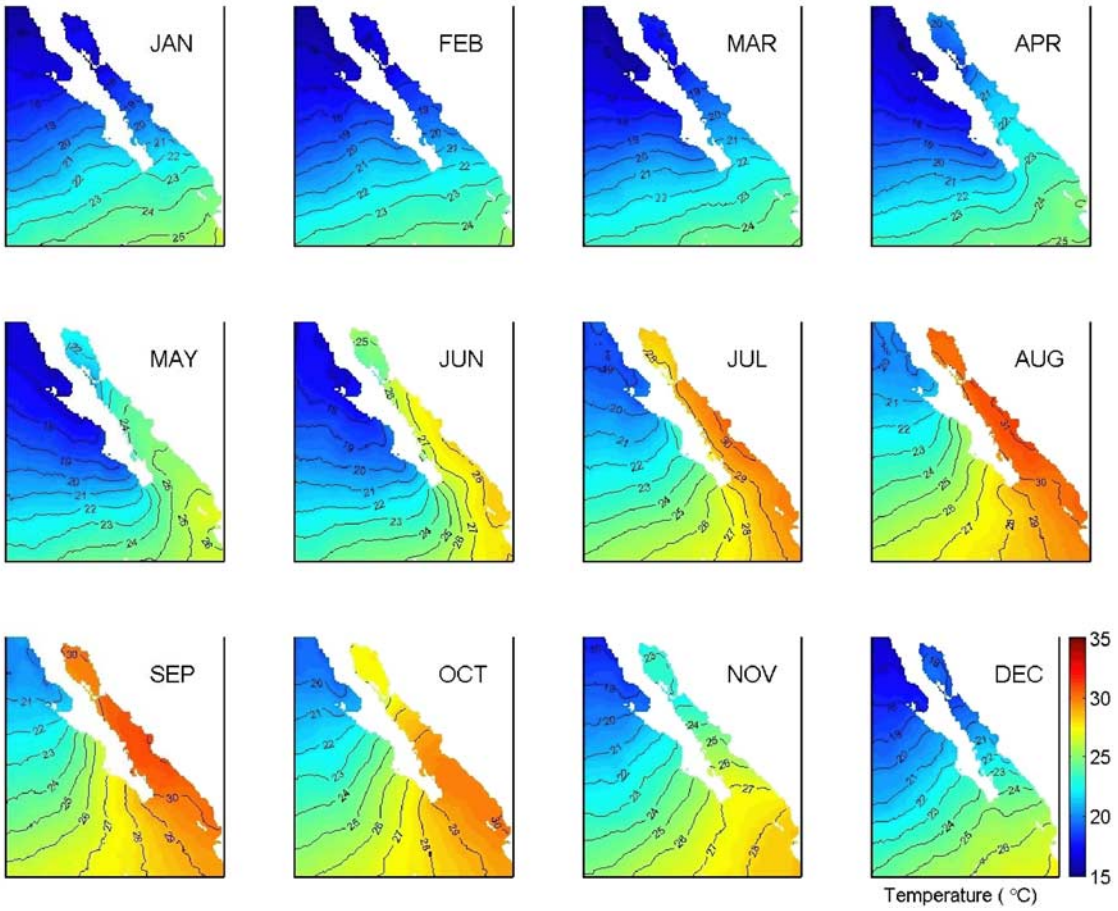

Figure 2. Monthly mean sea surface temperature of the Gulf of California, from the daily 9 km Pathfinder SST time series from 1985 to 1999, based on the "JPL AVHRR Pathfinder Global 9 km SST Climatology" (http://podaac.jpl.nasa.gov/climatology).

[8] Indeed, images like those in Figure 3 provoke questions as to whether there are currents associated with the mesoscale structures, how strong and deep they are, and what is their effect on the advective heat flux estimates. In particular, large eddies seem to be a characteristic of the entrance and southern Gulf areas, and the little available data indicate that they can be quite deep (>1000 m) [*Fernández-Barajas et al.*, 1994; *Collins et al.*, 1997; *Emilsson and Alatorre*, 1997; *Pegau et al.*, 2002; *Amador-Buenrostro et al.*, 2003; *Figueroa et al.*, 2003; *Zamudio et al.*, 2007, 2008]. Numerical models indicate that the main generating mechanism of these eddies is the interaction of the poleward Mexican Coastal Current and coastal trapped waves with coastal capes and ridges.

[9] In order to assess the relative importance of the meteorological and oceanographic causes of the Gulf of California SST evolution during the NAM onset and in its mature phase, two 14-day oceanographic cruises (in June and August 2004) were made in the entrance and southern portion of the GC, focusing on the spatial and temporal variability of the thermohaline structure and currents and on the air-sea interaction.

[10] The objective of this article is to describe the variability of the velocity and hydrographic fields in the entrance to the GC, as observed during the first NAME cruise, and to assess the effects of that variability on water column heat content and on advective heat flux estimates. To provide a three-dimensional description of the velocity and hydrographic fields that would include the characteristics of the mesoscale structures, a grid of sampling stations of unprecedented density (for the GC) was sampled (Figure 1). In addition, in order to evaluate the evolution in time, part of the grid was repeated with a separation of 1 week.

2. Data and Methods

2.1. Satellite Data

[11] As an aid in designing the ship sampling strategy and to obtain a larger-scale space and time perspective, the evolution of the sea surface temperature (SST) in the Gulf of California was monitored using 1 km × 1 km AVHRR data from NOAA-12, NOAA-16, and NOAA-17 satellites. These data were collected at CICESE's land station in La Paz, Baja California Sur, starting in May 2004 and for the duration of the NAME. In addition, automatic monitoring software was developed by *Cabrera et al.* [2006] to provide twice-daily SST images from GOES and MODIS and chlorophyll images from MODIS. The ocean wind from QuikScat (level 3, 25 km × 25 km resolution) was

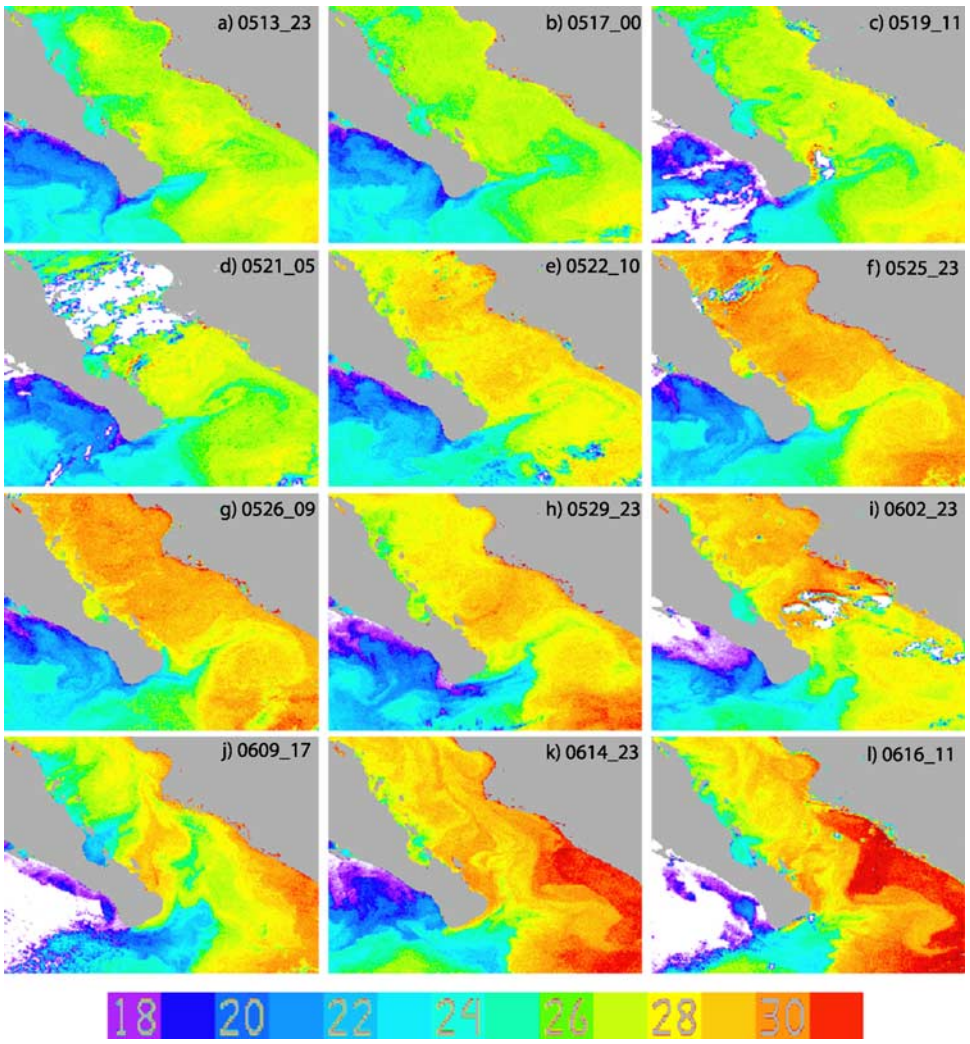

Figure 3. Selected AVHRR images (1 km × 1 km) from NOAA-12, NOAA-16, and NOAA-17 satellites from 13 May to 16 June 2004. The NAME-1 cruise dates (5 June to 17 June) fall within the last four images.

monitored for the same interval (http://podaac.jpl.nasa.gov/quikscat/qscat_news.html).

2.2. Hydrography and Current Data and Methodology

[12] The NAME-1 cruise was carried out on board the R/V *Francisco de Ulloa* from 5 June to 18 June 2004, in the portion of the southern GC shown in Figure 1. The vertical distributions of temperature, salinity, and currents were obtained in 174 oceanographic stations in 11 across-gulf Sections (Figure 1; Table 2). During stage 1 of the cruise, sections Z, X, and A to F were sampled, and in stage 2 a repeat of sections A to C was made (these sections were called A2, B2, and C2). Sections X and Z were a last-minute addition to the original cruise plan, in order to sample important features revealed by the satellite imagery (Figure 3). The spacing between stations within a section was ~10 km, except in sections F and C2, where it was ~20 km. The spacing between sections was between 30 and 40 km.

[13] The thermohaline profiles to 1500 m (or to ~5 m above the bottom if shallower) were measured with a factory-calibrated CTD (SeaBird SBE-911 plus), with primary and secondary sensors and with sampling rate of 24 Hz. The data were processed and averaged to 1 dbar as documented by *Godínez et al.* [2006]. Salinity (S) was calculated with the Practical Salinity Scale 1978. The potential temperature, θ (°C), and the density anomaly, γ_θ (kgm^{-3}), were calculated according to *UNESCO* [1991].

[14] The velocity profile was measured with a 300 kHz RDI Lowering Acoustic Doppler Current Profiler (LADCP) attached to the CTD protection frame. The absolute velocity profiles were obtained with the methods described by *Visbeck* [2002]. The sampling bins were 8 m deep.

[15] In order to remove unwanted variability in the θ and S vertical cross sections, an objective analysis technique was used. The fields of potential temperature and salinity were first averaged to 5 dbar, and then objectively mapped onto the original sampling grid using a Gaussian covariance function with length scales Lz = 50 dbar in the vertical and Lx = 70 km in the horizontal, which is about twice the local Rossby Radius of deformation and twice the wavelength of semidiurnal internal waves [*Beier*, 1997; *Filonov and Lavín*, 2003].

Table 1. Classification of Water Masses in the Gulf of California[a]

Water Mass	Abbreviation	S	T (°C)
Gulf of California Water	GCW	>34.9	≥12
Tropical Surface Water	TSW	<34.9	≥18
California Current Water	CCW	≤34.5	12 ≤ T ≤ 18
Subtropical Subsurface Water	StSsW	34.5 < S < 35	9 ≤ T ≤ 18
Pacific Intermediate Water	PIW	34.5 ≤ S < 34.8	4 ≤ T < 9
Pacific Deep Water	PDW	>34.5	<4

[a]*Lavín and Marinone* [2003]; *Castro et al.* [2006].

[16] Lagrangian surface currents were measured with ARGOS drifters of the SVP design, with a 10 m Holey sock centered at 15 m. Launchings were made from commercial ferries and from the R/V *Francisco de Ulloa* during the cruise. The data were cleaned and interpolated at 6-h intervals as described by *Hansen and Poulain* [1996].

2.3. Meteorological Data and Surface Heat Fluxes

[17] A set of meteorological instruments was installed on board the ship (http://data.eol.ucar.edu/codiac/dss/id=82.105), at a height of 9 m above the water surface, sampling at 2 Hz. Using these data, the sensible and latent heat fluxes were calculated using a bulk method [*Smith*, 1988]. These calculations were based on 20 min averages of air temperature, humidity, and wind speed for each period that was centered by an available bucket SST measurement.

[18] The net heat flux across the sea surface (Q, Wm^{-2}) is

$$Q = Q_s + Q_b + Q_h + Q_T,$$

where Q_s is the net solar (short wave) radiation, Q_b is the back (long wave) radiation, Q_h is the latent heat flux and Q_T is the sensible heat flux. Four values per day of Q_s and Q_b were obtained from the NCEP Reanalysis (data provided by the NOAA/OAR/ESRL PSD, Boulder, Colorado, USA, from their Web site at http://www.cdc.noaa.gov/) for the area covered by latitudes 22–25°N and longitudes 110–107°W. Direct observations of Q_s and Q_b in the GC entrance by *Zuidema et al.* [2007] in July and August 2004 in the GC entrance are in good agreement with the Reanalysis-derived values (averages: 241 versus 235 and −57 versus −56 Wm^{-2}, respectively).

3. Results

3.1. SST From Satellite Data

[19] The evolution of the SST in the southern GC prior and during the NAME-1 campaign is shown in Figure 3. In general, the lowest temperatures in these images (∼17–18°C) were found on the Pacific side of the peninsula and adjacent to it; these cold waters were identified with CCW. The highest temperatures (∼26–30°C) were found inside the Gulf, on the mainland shelf. On the peninsula side of the GC, there were isolated zones of low temperatures (∼23–26°C), e.g., in and off La Paz Bay (location in Figure 1).

[20] By late May, a sharp SST front was established between the cold CCW and the warm water in the Gulf entrance (GCW or TSW). From the second week of May (Figure 3a), tongues or filaments of cool water from the California Current seemed to intrude into the Gulf (Figure 3a). Initially these filaments were ∼20 km wide and had temperatures between 19°C and 21°C. They advanced from south of the tip of the peninsula directly across the Gulf entrance, almost normal to the Gulf axis (Figures 3a, 3b, and 3c). Their length, as measured from the peninsula, varied from ∼20–40 km (Figure 3a) to almost the distance to the mainland coast (Figures 3b–3d). The end of the intrusion developed a mushroom shape, with a cyclonic eddy in the north and an anticyclonic eddy in the south. After 22 May (Figure 3e) these features seemed to weaken, although the anticyclonic eddy appeared to stretch southeastward parallel to the mainland coast. In the subsequent images, (Figures 3f and 3g), this relatively cool (∼26°C) feature marked an anticyclonic eddy of ∼60 km diameter, which seemed to have decayed by 2 June after interacting with the mainland coast (Figures 3h and 3i).

[21] At the same time that the anticyclonic eddy developed and decayed (Figures 3f–3k), warm water (27–28°C) seemed to flow out of the Gulf as a narrow coastal jet attached to the tip of the peninsula. Also, the images from 2 and 9 June (Figures 3h and 3i) show that the intrusion of cool water intensified and veered toward the Gulf's interior. These conditions remained for several days (the NAME-1 cruise was underway on these dates), with the cool intrusion rapidly stretching for several tens of kilometers toward the interior of the Gulf (Figure 3j).

[22] A relevant feature of the SST images was the apparent invasion of warm water (≥29°C) from the SE along the mainland coast, starting between 2 and 9 June (Figures 3i and 3j). By 14–16 June (Figures 3k and 3l) the warm intrusion was ∼60 km wide and had the highest temperatures in these images, between 30°C and 31°C. This intrusion appeared to be associated with the stretching of the cool anomaly toward the GC interior. The offshore thermal front marking the warm coastal intrusion developed large meanders (Figures 3k and 3l).

3.2. Wind Field

[23] The 7-day average of wind velocity from QuikScat for the period 1 May to 27 June (Figure 4) showed that the wind inside the Gulf was northwesterly during the first week of May, while on the Pacific it was northwesterly during the entire period. As the wind over the Pacific side passed the tip of the peninsula (∼23°N), it turned cyclonically so that inside the Gulf the wind became south-southeasterly (Figures 4b–4g).

Table 2. Dates of CTD-LADCP Casts Performed in the R/V *Francisco de Ulloa* in the Gulf of California, June 2004[a]

Day (June 2004)	Section	Casts
	Stage 1	
5–6	X	1–13
6–7	Z	14–24
7–8	A	24–41
8–9	B	42–59
10–11	C	60–76
11–12	D	78–93
12–13	E	94–109
13–14	F	111–117
	Stage 2	
14–15	A2	118–135
16–17	B2	136–153
17	C2	154–161
18	LPB	162–174

[a]LPB is La Paz Bay.

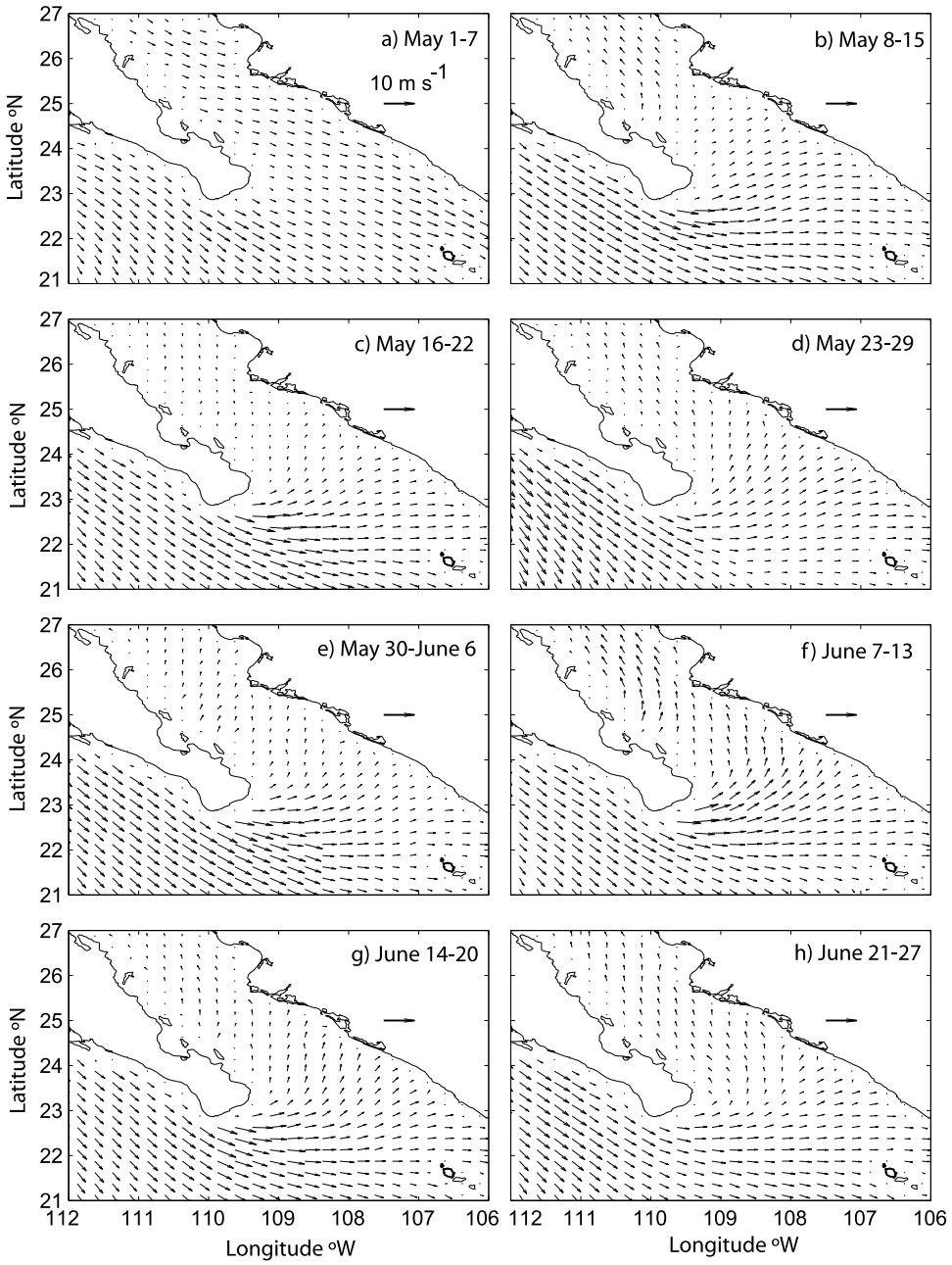

Figure 4. Seven-day averages of wind velocity from QuikScat, from (a) 1–7 May, (b) 8–15 May, (c) 16–22 May, (d) 23–29 May, (e) 30 May to 6 June, (f) 7–13 June, (g) 14–20 June, and (h) 21–27 June.

[24] The ship wind velocity observations are shown as 20 min averages and separated into the two stages in Figures 5a and 5b. Overall, the ship winds support the pattern of wind flow suggested by the satellite data as described above. There is however, more variability, as may be expected from the different sampling schemes. There was a general agreement between the two stages, showing a southerly southeasterly wind circulation pattern, with some variability close to the coast, probably associated with the breeze system. During stage 1, the wind was southerly and strong ($\sim$10 ms^{-1}) in the central part of section Z and weaker in section X than in section Z. In sections A, B, and C the wind was southeasterly and again stronger in the center of the Gulf than near the coasts. By contrast, the wind in section D was northwesterly and weaker in the central than in the lateral sectors. In section E the wind was weak and souther-southeasterly, except off Bahía de La Paz, where the wind was strong and southerly; this may be a local effect. In section F the wind was also weak, and southerly. During stage 2, the southeasterly wind pattern remained (Figure 5b), although weaker in A2 and B2 as compared to A and B.

3.3. Hydrography

[25] Figure 6 shows the θ-S diagrams of all the stations made during cruise NAME-1, separated by sections; the

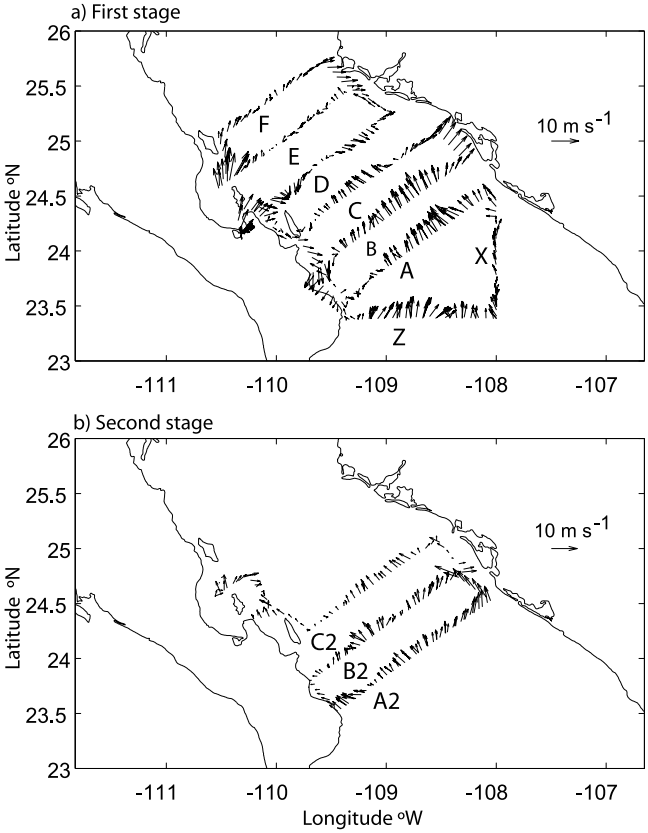

Figure 5. Wind velocity from ship data during cruise NAME-1. Twenty-minute data are shown for (a) first stage, 5–14 June 2004, and (b) second stage, 14–18 June 2004.

water mass classification of Table 1 is marked by straight lines. The average diagram is shown in Figure 6a; it was made with $\overline{S} \pm 1$ s. d., where the mean was calculated in θ bins of 0.5°C. There was a sharp increment in the dispersion of the salinity (Figure 6a) for potential densities below γ_θ = 26.5 kgm^{-3} (depths above ~250–300 m); this isopycnal (marked in black in Figure 6) was within the StSsW. This dispersion was due to the simultaneous presence, in the upper layers, of three water masses (CCW, TSW, GCW) in a relatively limited area.

[26] In the θ-S diagrams of the individual sections (Figures 6b–6l), the traces from profiles containing some water with salinity ≥35 are marked in black. The Z and X sections in the entrance contained mostly TSW and CCW (Figures 6b and 6c). In the six sections inside the Gulf (A–F, Figures 6d–6f), there was a striking separation of the stations with GCW and those without it, and this separation also corresponded to different geographical locations: the stations with high-salinity GCW were in the western side, while the stations with low-salinity CCW and TSW were on the eastern side. In sections D, E, and F (Figures 6g–6i) there was a clear separation between GCW and TSW, with almost no trace of CCW.

[27] The θ-S diagrams for stage 2 sections A2, B2, and C2 (Figures 6j–6l) show important hydrographic changes in the week between the two stages, with SST increasing by ~2–3°C. Sections A2 and B2 showed an invasion of warmer TSW, while the GCW in the western side was much less evident than in the first stage.

[28] The vertical sections of θ and S are shown in Figures 7 and 8, respectively. The structures of θ and γ_θ were very similar; therefore the latter are not shown. The strongest stratification was above 100 dbar, between 15°C (25.5 kgm^{-3}) and 28°C (23 kgm^{-3}). The areas of surface temperature minimum described in the satellite images were associated with isotherms rising to the surface; this feature seemed to shift from the western side in section A, to the center in B, and to the east side in C, it was less apparent in D and E and was absent in F. In sections A and B, at ~30 km from the peninsula coast the 17–27°C isotherms showed this isotherm doming (Figure 7d): the 24°C rose from 30 dbar to ~5 dbar, while the isotherms between 25 and 27°C reached the surface.

[29] The isotherms (and isopycnals) showed a general downward tilt toward the mainland, so that water at a given depth was warmer (less dense) on the mainland side than on the peninsula side. Below 200 dbar, the isolines showed an uplifting in the central section, leading to a general doming. The largest central uplifting occurred in section F where the 10°C isothermal was ~90 dbar higher in the center than in the sides (Figure 7h).

[30] The largest variability of S was in the upper ~200 dbar (Figure 8), although below ~300 dbar there was a ~70 dbar deepening of the isohalines on both sides, corresponding to the doming of the isotherms described above. As observed in the description of the θ-S diagrams, sections Z, X, A, and B showed a large influence of TSW and CCW; their 10–130 dbar layer was dominated by a low-salinity intrusion (S < 34.7). Section Z (Figure 8a) shows two cores with S ≤ 34.6, one close to the peninsula, and another at the other extreme of section Z. The latter intrusion seemed to extend, along section X, to the mainland shelf. In section A (Figure 8c), salinities below 34.6 were found almost throughout the section, from the surface to 100 dbar, and there were two low-salinity cores (≤34.5).

[31] In section B (Figure 8d), the 34.5 isohaline was found between 10 and 70 dbar in a band ~100 km wide, and a core of minimum salinity ~34.2 was at a distance of ~60 km from the peninsula at ~40 dbar. Between the peninsula and the low-salinity intrusion, salinity was generally high (≥34.9), and the area occupied by the high salinity water (GCW) increased toward the interior of the Gulf (Figures 8c–8h). In section Z (Figure 8a), attached to the tip of the peninsula there was a small intrusion of high salinity (≥34.8) water between 20 and 150 dbar. This intrusion was probably an extension of the high-salinity cores of 35.0 at ~50 dbar in sections A and B. By section B, the GCW covered a surface band some 70 dbar deep and ~45 km wide, with salinities from 35 to 35.3.

[32] In sections C to F (Figures 8e–8h), most of the area above 200 dbar was occupied by GCW with salinity ≥34.9 (and up to 35.3), while lower values were restricted to the mainland shelf. The exception was the small salinity minimum at ~50 m in section C close to the peninsula, which appeared to migrate toward the mainland in section D; this minimum caused the 34.9 isohaline to exhibit large depth variations. In sections A to E, the strong, almost vertical haline front between the salty GCW and the low-salinity water caused the 34.9 and 34.8 isohalines to reach the surface.

[33] The sections A2, B2, and C2 (Figure 9) show the notable hydrographic changes that took place in only 1

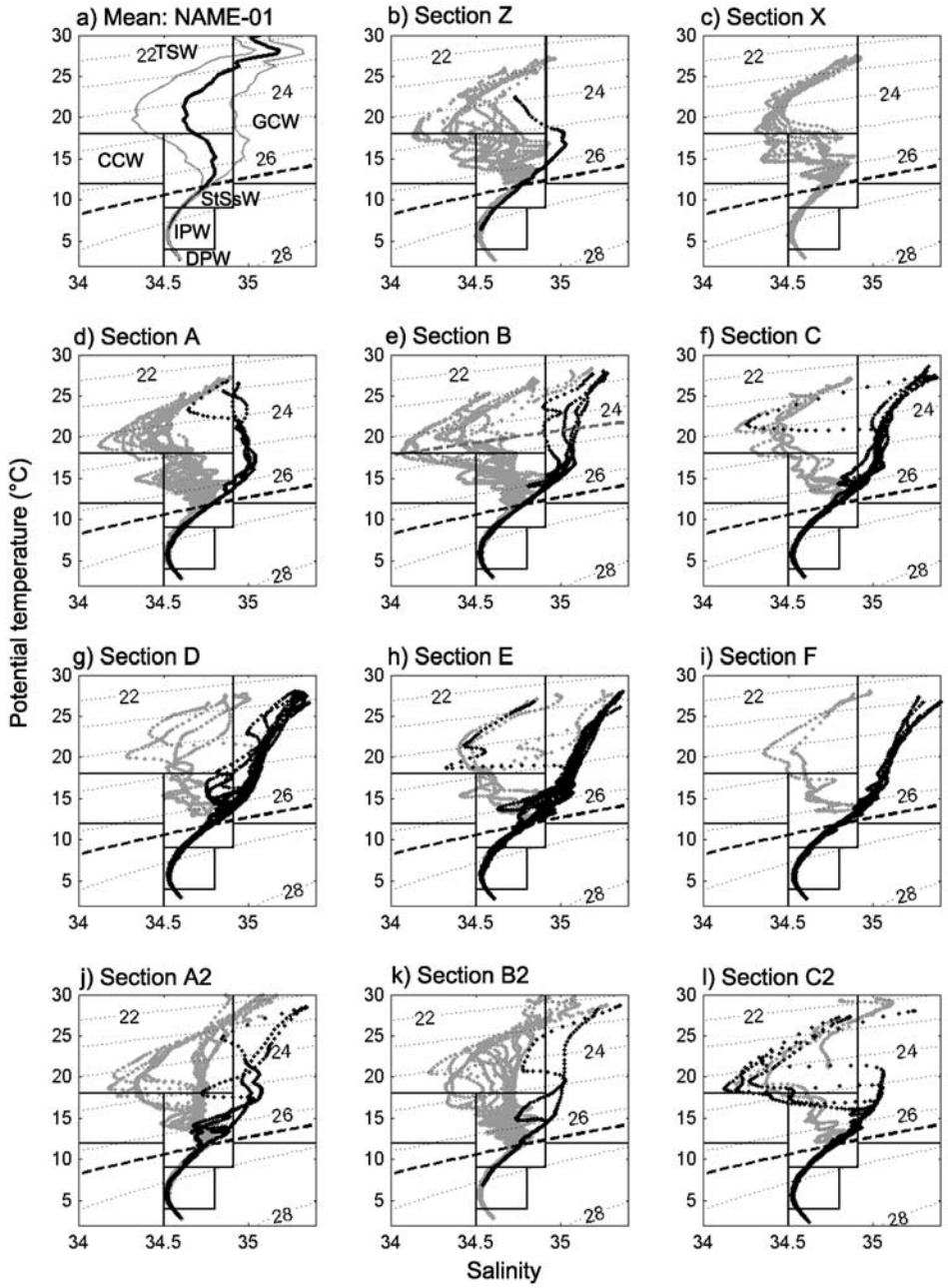

Figure 6. NAME-1 θ-S diagrams, with the classification of the water masses found in the Gulf (Table 1). (a) Average ±1 standard deviation, calculated for θ bins of 0.5°C. Diagrams by section: (b–i) first stage, (j–l) second stage. Dashed black line, isopycnal of $\gamma_\theta = 26.5$ kgm^{-3}. Solid line gray (Figure 6e only), isopycnal of $\gamma_\theta = 24.55$ kgm^{-3}. Black traces indicate stations containing GCW; gray traces indicate stations containing CCW and TSW. See Table 1 for waters masses nomenclature.

week. The SST increased by ~3–4°C (from 27 to 31°C) in the eastern side of section A, and by ~2°C in section B (Figures 9a and 9b). In sections A2 and B2 (Figures 9d and 9e), the salinity distribution showed less influence of low-salinity water (≤34.5) from the CCW, but a larger presence of tropical water (34.6–34.7).

[34] The salinity distribution in section C2 (Figure 9f) changed substantially, both as compared to A2 and B2 and to the situation in stage 1. While in sections A2 and B2 GCW (>34.9) was present in a very shallow surface layers in the central and eastern sides, in C2 there was also a nucleus of GCW attached to the peninsula, between 50 and 150 m, and covering almost half of the section. This squeezed the low-salinity core into a layer between 10 and 50 m depth that covered from side to side of the section.

3.4. Currents (LADCP)

[35] Figure 10 shows the stage 1 current observations from the LADCP, depth-averaged as indicated (note the changes in velocity scale); data were collected to 1500 m,

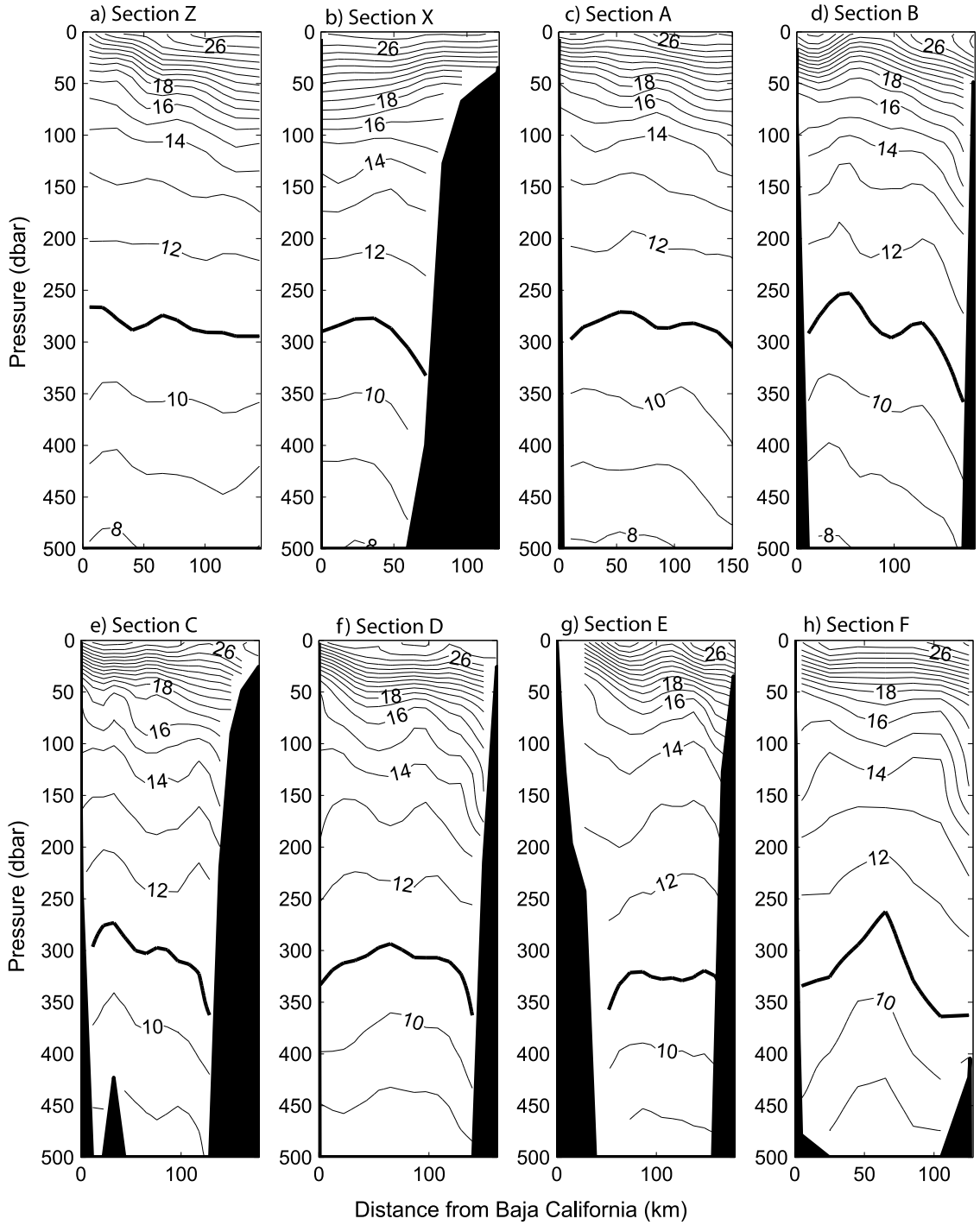

Figure 7. Vertical sections of potential temperature (°C) during the first stage of cruise NAME-1. The contour interval is 1°C, and the thick line is the 11°C isotherm.

but only the top 1000 m are shown. The main features in the top 50 m (Figure 10a) agreed very well with the geostrophic velocity calculations (see auxiliary material)[1]: (1) on the mainland side, a very intense (up to 0.55 ms^{-1}) northwestward coastal current, which appeared to narrow with distance into the Gulf; (2) weak currents and convergence in the central zone, (3) an outgoing coastal flow on the peninsula side, which was narrow in sections Z, A, and B, undefined in sections C and D, and covered half of the Gulf width in sections E and F. The surface current pattern was

[1]Auxiliary materials are available in the HTML. doi:10.1029/2008JC004896.

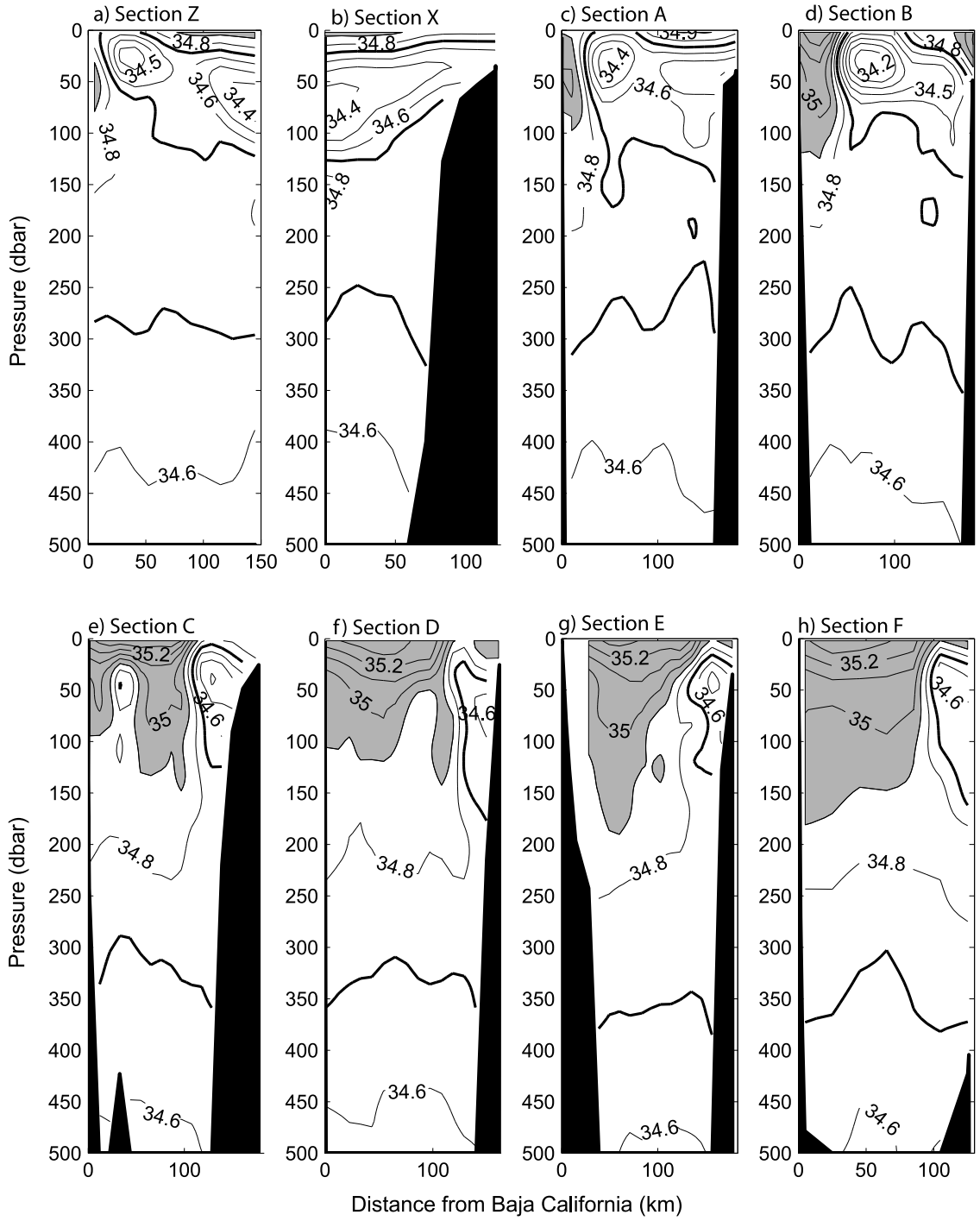

Figure 8. Vertical sections of salinity during the first stage of cruise NAME-1. The contour interval is 0.1, the thick line is 34.7, and the shaded areas have salinity $\geq$34.9 (indicating GCW).

maintained in the deeper layers, although with slower speeds.

[36] In section Z (Figure 10a) the surface flow changed from weak (0.15–0.20 ms^{-1}) and to the south close to the tip of the peninsula, to a stronger (0.30–0.52 ms^{-1}) northward flow in the eastern half of its width; the non-divergent inflowing transport to 1000 m was 6 Sv. In section X, surface currents had variable direction and were weaker ($\sim$0.15–0.25 ms^{-1}) than in section Z, and although no inflowing coastal flow was apparent at the surface, it was present in the 50–500 m layer (Figures 10b–10d); the inflowing transport to 1000 m was 2 Sv. In sections A and B surface currents were mostly to the northwest, with an offshore weakening from >0.4 ms^{-1} in section A (>0.6 ms^{-1} in section B) in the east to <0.25 ms^{-1} offshore; close to the peninsula the surface flow was to the southeast,

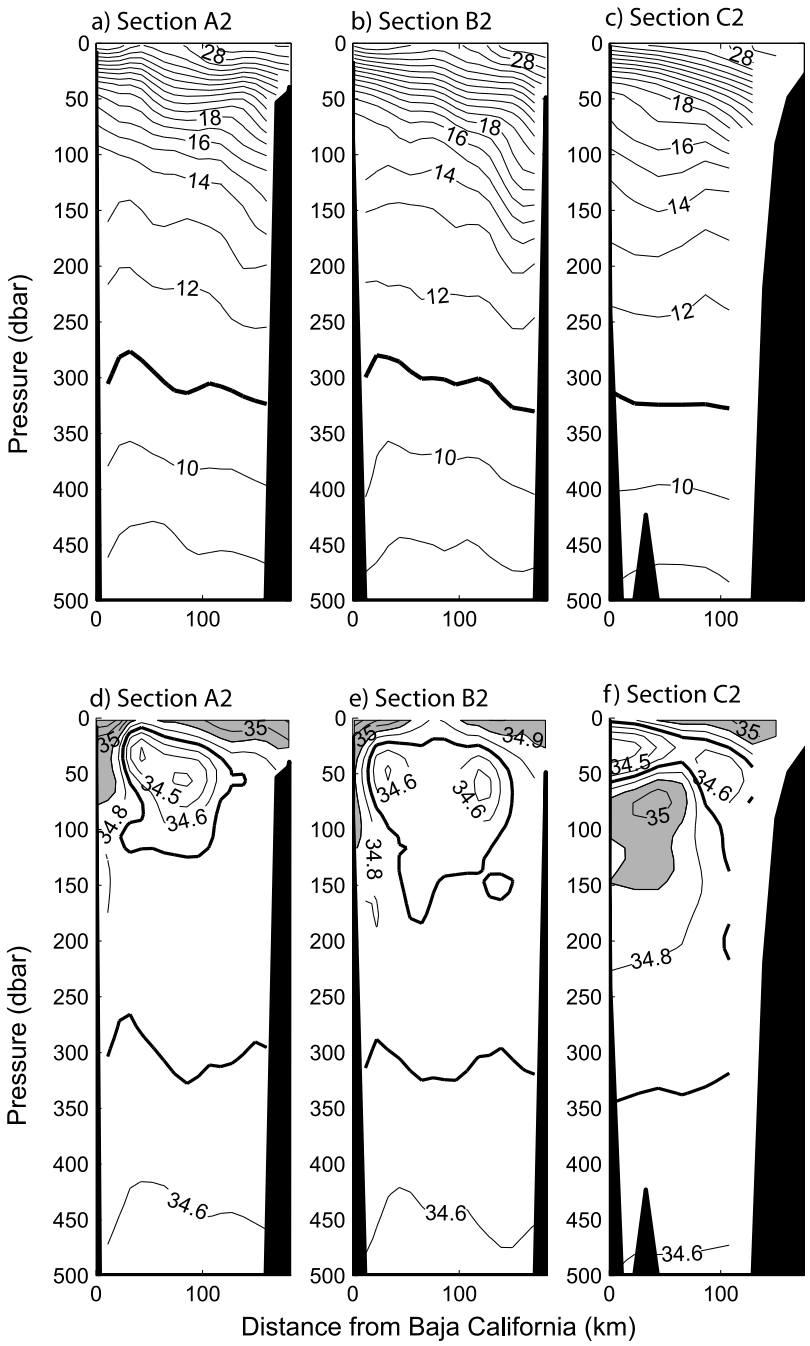

Figure 9. Vertical hydrography sections during the second stage of cruise NAME-1. (a–c) Potential temperature (°C), the contour interval is 1°C, and the thick line is the 11°C isotherm. (d–f) Salinity, the contour interval is 0.1, the thick line is 34.7, and the shaded areas have salinity ≥34.9 (indicating GCW).

at ∼0.30 ms^{-1}. The inflowing transport in section A was 8 Sv, which balances quite well with the sum of the transports in sections X and Z, and shows that most of the transport into the GC during the observations was due to currents in section Z.

[37] In section C, the inflowing surface current was very similar to that in A and B, with a large proportion of the area with speeds ∼0.4 ms^{-1}. The southeastward surface flow close to the peninsula was also present with speed ∼0.20 ms^{-1}. The pattern changed in section D, with most of the section showing very weak surface current, except in the eastern side where the northwest inflow was present. In sections E and F the southeastward surface flow covered most of the western part (∼0.2–0.40 ms^{-1}). The northwestward coastal current in the mainland side is very intense in sections D, E, and F, with maximum speeds of 0.5 ms^{-1}, 0.65 ms^{-1}, and 0.64 ms^{-1}, respectively. A region of convergence is suggested in the central part of section D.

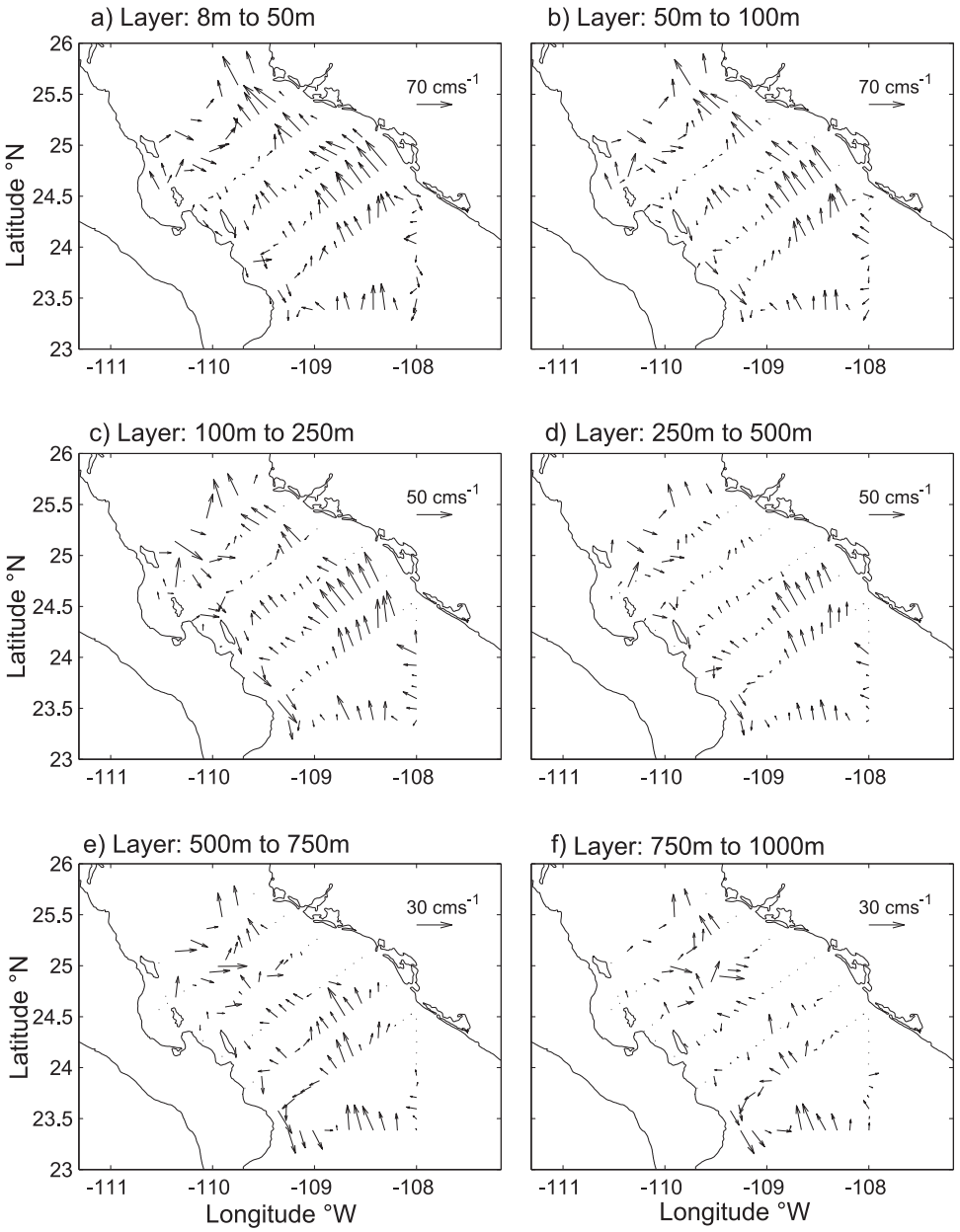

Figure 10. First stage current velocity vector from the LADCP, averaged in the intervals indicated: (a) 8 to 50 m; (b) 50 to 100 m; (c) 100 to 250 m; (d) 250 to 500 m; (e) 500 to 750 m; (f) 750 to 100 m. The scale vector is shown in the top-right of each plot; note that it varies with depth.

[38] The current velocity pattern seen in the surface remains almost unchanged down to 250 m (Figures 10b and 10c). The strong northward flow (0.20–0.30 ms^{-1}) in the offshore part of section Z, and the similarly strong inflow (0.15–0.40 ms^{-1}) in sections A and B remained strong down to 500 m, and were present, although weaker, down to 1000 m; this was also present in the geostrophic calculations (see auxiliary material). In the 250 to 500 m average (Figure 10c), the coastal jet on the mainland side had maximum speeds of ~0.35 ms^{-1}, 0.40 ms^{-1}, and 0.33 ms^{-1} in sections A, B, and F, respectively, while in the remaining sections the speeds were not as fast (0.1–0.2 ms^{-1}). The outgoing flow close to the tip of the peninsula is also detectable to 1000 m.

[39] The LADCP stage 2 sections A2, B2, and C2 were weaker and with more variable currents than in stage 1, although mostly inflowing (Figure 11). The outflow jet close to the peninsula remained, with speeds ~0.10 and 0.25 ms^{-1} down to ~500 m and with maximum (0.27 ms^{-1}) in the 100–250 m layer (Figure 11c). In a similar fashion as in sections A–C, the surface currents in A2–C2 (Figure 11a) increased from west to east, but with the difference that now the flow was mostly to the north-northeast, with speeds over 0.5 ms^{-1} in some stations. This surface pattern remained to ~500 m. In the eastern half of the two deepest layers in sections B2 and C2 (Figures 11e and 11f), an anticyclonic eddy was suggested.

[40] The flow pattern from the ARGOS drifters during the NAME-1 cruise (Figure 12) agrees very well with LADCP

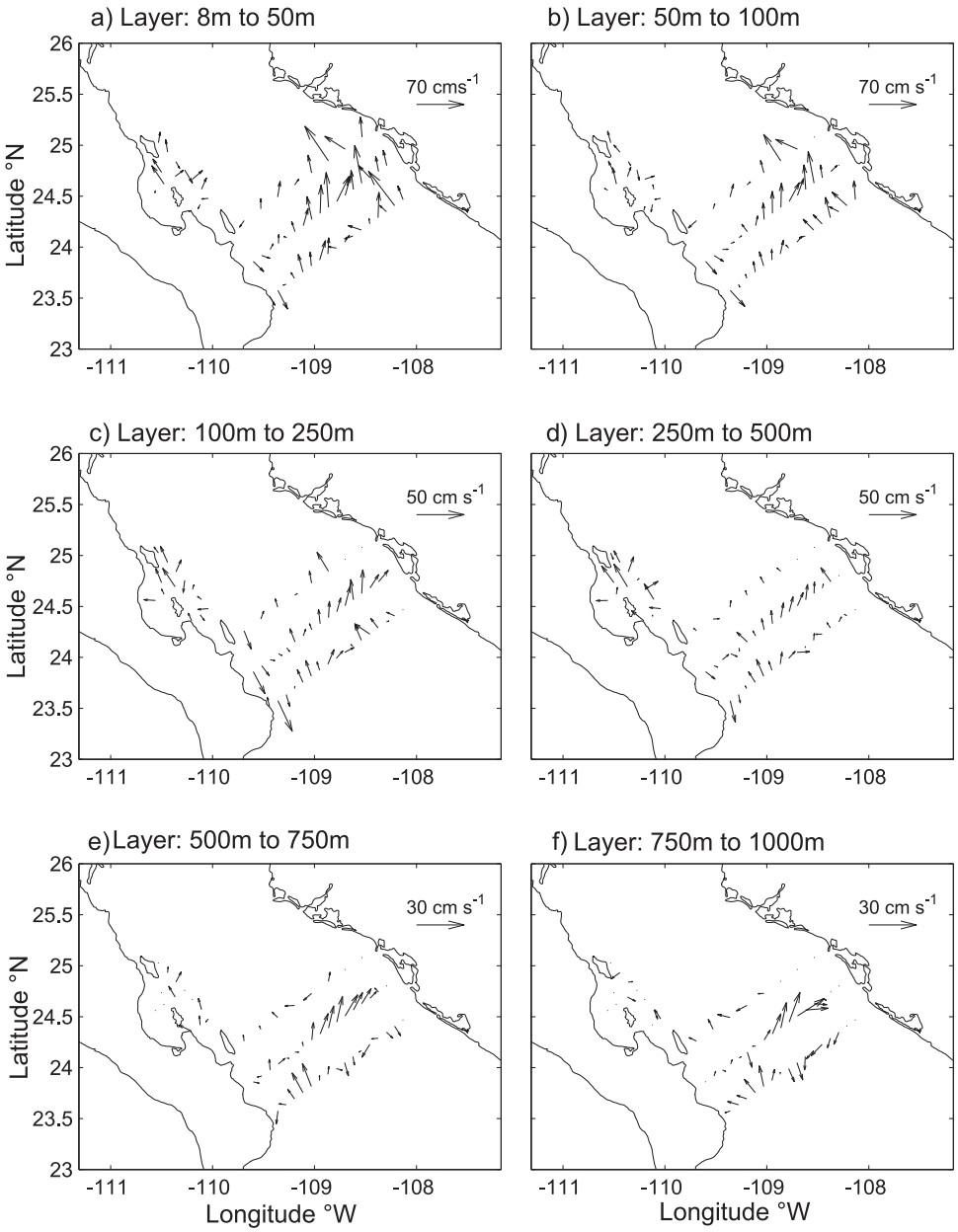

Figure 11. Second stage current velocity vector from the LADCP, averaged in the intervals indicated: (a) 8 to 50 m; (b) 50 to 100 m; (c) 100 to 250 m; (d) 250 to 500 m; (e) 500 to 750 m; (f) 750 to 100 m. The scale vector is shown in the top-right of each plot; note that it varies with depth.

and geostrophic velocities: (1) fast (0.5–0.7 ms^{-1}) inflow in a narrow band parallel to the mainland coast, (2) near stagnation in the central and western parts of the inner sections indicating convergence, and (3) weak outflow off the peninsula. The pattern continued until at least 24 June.

4. Discussion

4.1. Surface Currents, Temperature, and Salinity

[41] The data collected during the NAME-1 cruise provided a detailed three-dimensional description of the circulation and hydrography at the entrance of the GC, including changes in a week's time. Of particular interest to the NAME, since this is the period in which the SST of the GC starts to increase rapidly, account can be given of the relationship between circulation and SST.

[42] The AVHRR images (Figure 3) illustrate the great space-time variability present in the entrance of the GC at this time of the year, with a proliferation of mesoscale structures (fronts, eddies, meanders, jets, etc.) that affected the SST distribution; the largest structures were (1) the cool anomaly that appeared to intrude across the entrance, (2) the warm water intrusion attached to the mainland coast, and (3) a warm and narrow band of warm water exiting the Gulf attached to the tip of the peninsula. These features appear to be recurrent, occurring most years.

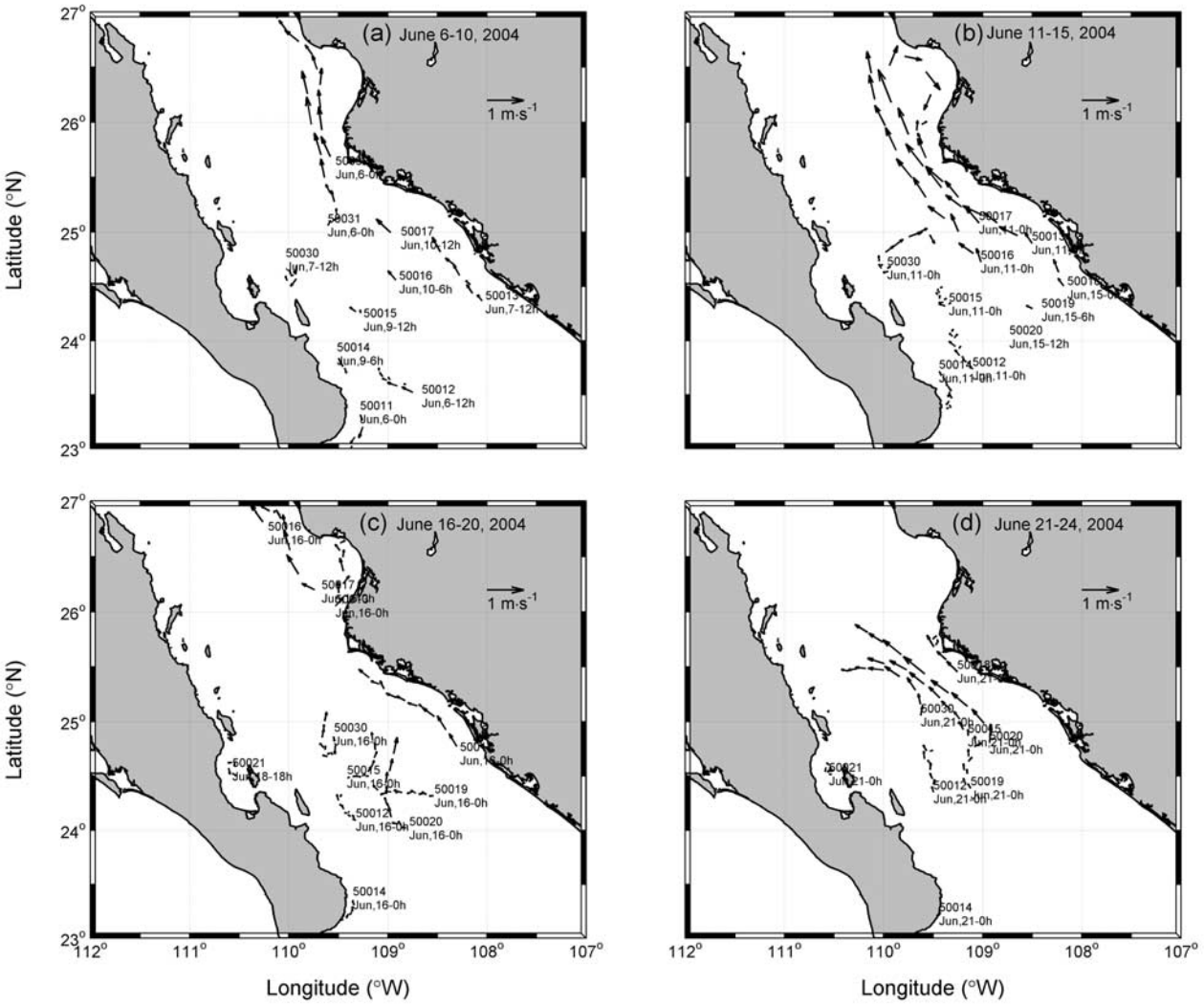

Figure 12. Surface velocity vectors from ARGOS drifters during the NAME-1 cruise: (a) 6–10 June, (b) 11–15 June, (c) 16–20 June, (d) 21–24 June. Starting date/time (UT) and drifter serial number are shown. Data every 12 h.

[43] Figure 13 shows the temperature and salinity distributions in the surface and at 20 m depth, together with the LADCP velocity vector averaged in the upper 24 m ($\mathbf{V}_{24}$). The temperature at 20 m shows a richer pattern than the SST, including a band of cool water attached to the peninsula, caused by the tilting isotherms seen in the vertical sections (Figure 7), which is intensified close to the peninsula, probably by coastal upwelling.

[44] $\mathbf{V}_{24}$ strongly suggests an intrusion through section Z, which then veered and flowed into the GC. However, the fastest currents did not occur on the cool anomaly, but to the east or northeast of it, on warmer water. The occurrence of fast currents on filament flanks has been observed in the California Current [*Flament et al.*, 1985; *Kosro and Huyer*, 1986] and in the Gulf of California [*Navarro-Olache et al.*, 2004]. The reason for this is that the isotherms (and isopycnals) were domed under the SST minimum (Figure 13a, 13c), and therefore the geostrophic velocity (shown in auxiliary material) was weak over the SST minimum and strong on the sides. Therefore the interpretation of the cool anomaly is not that it was a cool jet, but a frontal area caused by the lifting of the isotherms by a deep structure. The sequence of AVHRR images prior to the cruise (Figures 3g–3i) suggests that such structure was an anticyclonic eddy, which was decaying by the time sections Z and X were sampled (Figure 3i).

[45] The details of mesoscale generation processes in this area are beyond the objectives of this study, but of the many possibilities [*Federov and Ginsburg*, 1986], frontal instability and localized wind impulses seem to be two of the likely generation mechanisms in the GC entrance area, since sharp SST fronts are ubiquitous (Figure 2), and between May and June the wind turns cyclonically into the Gulf (Figures 3 and 4). Numerical models suggest that instability of the poleward Mexican Coastal Current is a very important eddy-generating mechanism in this area [*Zamudio et*

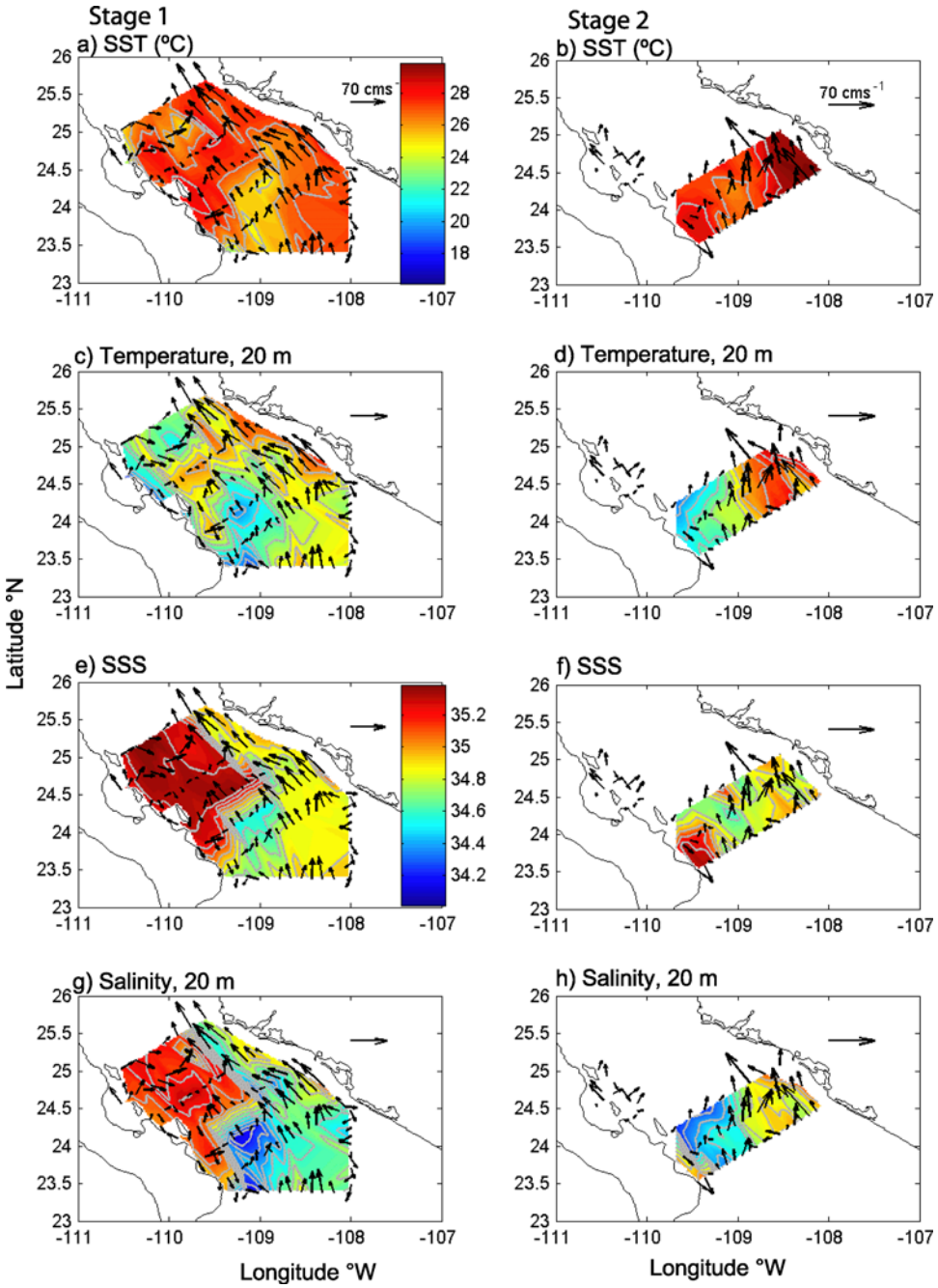

Figure 13. Horizontal distributions of ADCP velocity averaged in the upper 24 m ($\mathbf{V}_{24}$), overlaid on CTD temperature and salinity during the two stages of NAME-1 (5–14 June and 16–17 June 2004). (a) SST (°C) stage 1, (b) SST (°C) stage 2, (c) temperature at 20 m stage 1, (d) temperature at 20 m stage 2, (e) surface salinity stage 1, (f) surface salinity stage 2, (g) salinity at 20 m stage 1, (h) salinity at 20 m stage 2.

al., 2007, 2008], especially off the mainland coast. The AVHRR images (Figure 3) suggest that the anticyclonic eddy associated with the cool filament was generated in the offshore frontal area, rather than close to the mainland.

[46] The temperature distribution at the surface and at 20 m during stage 2 (Figures 13b and 13d) showed a clear warming, already described in section 3.3, especially close to the mainland side. There was a general SST increase of ~2°C relative to stage 1, while at 20 m depth the temperature increase was ~1.5°C. The rise in temperature was also apparent in the satellite AVHRR images of 14 and 16 June (Figures 3k and 3l), which also suggest that it was due to the northwestward intrusion of warm water along the mainland continental shelf. This warm water intrusion is probably due to the Mexican Coastal Current, and the isotherm advance seen in the SST climatology (Figure 2)

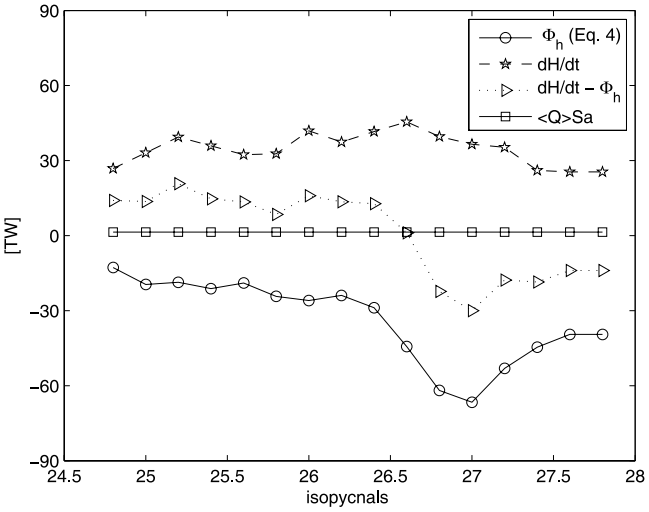

Figure 14. Heat balance terms (equation (1)) for the volume of the gulf corresponding to transects A, B, and C (first stage, 11 June) and A2, B2, and C2 (second stage, 15 June). dH/dt, stars. Divergence of the advective heat flux (equation (4)), circles. dH/dt − Div($\mathbf{F}_h$) triangles. Mean surface heat flux from bulk formulae (equation (3)), squares.

suggests that it is an annual phenomenon. A possible origin for the warm coastal current flowing into the GC is the reversal of the normally upwelling-favorable winds, as has been observed in the California coast [*Send et al.*, 1987] and in the Bay of Biscay [*Relvas and Barton*, 2002]. Also, *Zamudio et al.* [2008] suggested that in June 2004 the Mexican Coastal Current was strengthened by a particularly strong coastal trapped wave (CTW), which could be reflected in the warm intrusion. However, the geostrophic velocity sections (shown in auxiliary material) and the LADCP data (Figure 10) show that the coastal current was wider than one baroclinic Rossby radius of deformation (∼30 km in this area), and located far from the coast.

[47] The distributions of salinity at the surface and 20 m (Figures 13e and 13g) showed more contrasts than those of temperature, because of the sharp haline front between the GCW (S > 34.9) and the low-salinity water being advected into the GC by the inflowing coastal current, and the still lower salinity associated with the cool anomaly. The repeated salinity observation of sections A, B, and C during stage 2 (Figures 13f and 13h) show that the band of GCW that was attached to the peninsula in sections A, B, and C during stage 1 (Figures 13e and 13g) detached from the main body of GCW, and was replaced by fresher water.

[48] In most of the sampled area the general SST increase of ∼2°C was accompanied by an increase in surface salinity of ∼0.15. At 20 m depth the salinity close to the peninsula diminished, but it increased in the central sector and in the mainland shelf (by up to 0.2). This high salinity (>35) was apparent in the surface during stage 1 (Figure 13e) in the area where sections Z and X intersected; therefore it could be surmised that it was advected to A2−C2 by the inflow through section Z.

4.2. Heating and Heat Fluxes

[49] The results above suggest that much of the heating and salinity increase observed in the surface layers on the mainland side of the entrance to the GC was due to advection. We now investigate the case of heating by using the heat balance equation.

[50] Let H (J) be the heat content of a volume G of the Gulf of California

$$\mathrm{H} = \int\int\int_{\mathrm{G}} \rho \mathrm{C_p} \theta(\mathrm{x},\mathrm{y},\mathrm{z}) dxdydz, \tag{1}$$

where ρ is the density (kg m^{-3}), C_p (J kg^{-1} K^{-1}) is the heat capacity of seawater and θ is the potential temperature. The coordinates are: x along-gulf and positive toward the entrance, y across-gulf and positive toward the mainland, and z positive upward. The heat balance of volume G is

$$\mathrm{dH/dt} = \int\int\int_{\mathrm{G}} \mathrm{Div}(\mathbf{F}) dxdydz = \int\int_{\sigma} \mathbf{F}.\mathbf{n} ds, \tag{2}$$

where $\mathbf{F}$ (Wm^{-2}) is the heat flux through the entire boundary (σ) of G and $\mathbf{n}$ is a unit vector normal to the surface element ds of σ. Let $\mathbf{F}_h$ be the horizontal heat flux and let $\mathbf{F}_v$ be the vertical heat flux, so that

$$\mathrm{dH/dt} = \int\int_{\sigma} (\mathbf{F}_h + \mathbf{F}_v).\mathbf{n} ds \equiv \Phi_h + \Phi_v,$$

where Φ_h and Φ_v (W) are the area integrals of the horizontal and vertical heat fluxes, respectively.

[51] The volume G of the Gulf of California chosen to investigate the terms of the heat balance equation is bound in the vertical by sections A and C and the mainland and peninsular continental shelves and slopes, in the horizontal by the sea surface, and its lower boundary is an isopycnal surface γ_b (to be chosen later) through which $\mathbf{F}_v$ is negligible.

[52] The heating due to the vertical heat flux is

$$\begin{aligned}\Phi_v &= \int\int_{\sigma} \mathbf{F}_v.\mathbf{n} ds = \int\int_{\mathrm{Sa}} \mathbf{Q}.\mathbf{n} dxdy \\ &+ \int\int_{\gamma_b} \mathbf{F}_v.\mathbf{n} ds = \int\int_{\mathrm{Sa}} \mathrm{Q} dxdy = \langle \mathrm{Q} \rangle \mathrm{Sa},\end{aligned} \tag{3}$$

where $\langle Q \rangle$ is the average net surface heat flux and Sa is the sea surface area (Sa = 210 × 80 × 10^6 m^2) of volume G. The surface heat fluxes obtained as described in section 2.3 were averaged for the times when sections A, B, C, A2, B2, and C2 were made, giving

$$\begin{aligned}\langle \mathrm{Q} \rangle &= \langle \mathrm{Q_s} \rangle + \langle \mathrm{Q_b} \rangle + \langle \mathrm{Q_h} \rangle + \langle \mathrm{Q_T} \rangle = 257 - 64 - 103 - 5 \\ &= 85\,\mathrm{W\,m^{-2}}.\end{aligned}$$

This value is comparable to the 70 W m^{-2} obtained by *Zuidema et al.* [2007] in the GC entrance for the period 7 July to 11 August 2004. Therefore, for the area covered by the A, B, and C sections during the NAME-1 cruise, the heating due to vertical heat flux is $\langle Q \rangle$Sa = 1.4 TW.

[53] To calculate the rate of change of the heat content of volume G, equation (1) was evaluated using temperatures interpolated linearly (in time) to zero hours of days 11 and 15 of June 2004, based on the two samples collected during stage 1 and stage 2. This interpolation was necessary to

Table 3. Advective Horizontal Heat Flux (F_{GC}, 10^5 W m^{-2}) in the Gulf of California Entrance[a]

Section	Z + X	A	A2	B	B2	C	C2	D	E	F	Mean ± Standard Deviation
LADCP, June 2004	3.8 + .85	9.6	7.0	2.2	1.2	5.6	4.5	9.7	5.3	3.8	4.8 ± 3.0
Geostrophic. June 2004	7.3 + 0.75	6.3	3.8	7.8	6.6	4.6	1.3	8.1	5.8	4.4	5.7 ± 2.2
Geostrophic. May 1998		2.0		4.1		6.2					4.1 ± 2.1
Areas for LADCP	1.7 + 0.6	1.6	1.6	1.4	1.6	1.1	1.2	1.2	1.2	1.2	1.3 ± 0.32
Areas for Geostrophic	1.9 + 0.9	2.1	2.1	2.2	2.2	1.6	1.5	1.8	1.6	1.5	1.7 ± 0.39

[a]The integrations (equation (5)) with geostrophic velocity were made to 1500 m, and those with LADCP velocity to the $\gamma_b = 27.5$ isopycnal. The last two rows present the area (10^8 m^2) of the cross sections.

define with precision the time interval over which dH/dt was calculated. The values of H and dH/dt depend on γ_b, as shown in Figure 14 (stars). The plot of dH/dt shows that heating took place in the upper layers, from the surface to the 26.7 isopycnal; when taken to this isopycnal surface, the heating is ~45 TW. If dH/dt is calculated to deeper γ_b ($\geq$27.4), it decreases (to ~25 TW); which means that the Gulf lost heat in the deeper layers during this time period (diabatic and adiabatic). It is the latter value that is relevant for comparison with previous calculations, which were made to 400 m [*Castro et al.*, 1994] or to over 1500 m [*Mascarenhas et al.*, 2004].

[54] It is clear that such value of dH/dt could not have been caused by the 1.4 TW of surface heat flux; it must have been caused by advective lateral heat flux $\mathbf{F}_h$. We can obtain an estimate of its value from the heat balance equation (2), as *Castro et al.* [1994] did for the seasonal time scale:

$$\Phi_h = dH/dt - \langle Q \rangle Sa = 25 - 1.4 = 23.6\,\text{TW}.$$

However, in principle we have all the data needed to calculate directly the lateral heat fluxes and their divergence, as

$$\Phi_h = \int\int_{\sigma} \mathbf{F}_h.\mathbf{n}ds = \int\int_{A} C_p\rho(\mathbf{V}\theta).\mathbf{n}dydz + \int\int_{C} C_p\rho(\mathbf{V}\theta).\mathbf{n}dydz. \quad (4)$$

Here $\mathbf{V}$ is the LADCP current velocity with the mean of each cast removed, θ is the potential temperature, and $\mathbf{n}$ is a unit vector normal to the corresponding vertical surfaces A and C. These values of $\mathbf{V}$ and θ were interpolated linearly to zero hours of 13 June 2004, which is in the middle of the period used to calculate dH/dt. The vertical boundaries used for the integrals were the CTD stations on the two extremes of sections A and C, the upper boundary was the sea surface and the lower boundary was the γ_b isopycnal. The value of Φ_h depends on γ_b, as shown in Figure 14.

[55] The plot for Φ_h (Figure 14, circles) shows a net heat gain (convergence) by advection of ~10 TW when integrating to the 26.5 isopycnal. The value then increases to ~70 TW for $\gamma_b = 27$ before settling at ~38 TW for $\gamma_b \geq 27.4$. Taking the latter value (38 TW) for consistency with the dH/dt calculations, we see that it is larger than that obtained from the heat balance equation (23.6 TW). However, the calculation of (4) has large uncertainties, most of which stem from the fact that the integration was not performed on the entire cross sections but on the sampled areas. Thus the explanation for the increase in Φ_h for intermediate values of γ_b is not clear without looking at the vertical distributions of $\mathbf{V}$, θ, and $\mathbf{F}_h$ on each section. This uncertainty is also reflected in the difference dH/dt − Φ_h ≈13 TW (for $\gamma_b > 27.4$), which is one order of magnitude larger than the surface heat flux $\langle Q \rangle Sa = 1.4$ TW.

[56] Although the comparison of dH/dt against Φ_h should be made with caution because of the large errors associated with their calculation, the conclusion that the surface heat flux cannot explain the heating of the water column remains valid. This is in agreement with previous estimates of seasonal fluxes of heat and salinity [*Castro et al.*, 1994; *Beron-Vera and Ripa*, 2002; *Mascarenhas et al.*, 2004], and with the NAME study by *Zuidema et al.* [2007] The latter authors made a 5-week (7 July to 11 August 2004) time series of observations at a single point in the same general area sampled here; they found that the salinity decrease and temperature increase in the top 20 m of the water column observed during their observation period could not be explained by surface fluxes of heat and moisture. Therefore our data give credence to the suggestion of *Mitchell et al.* [2002] that the observed progression of the surface isotherms in climatological May–June into the GC is due to advection.

4.3. Advective Heat Flux at the Entrance

[57] One of the motivations for this study was to obtain a reliable value of

$$\alpha^{-1} \int\int_{\alpha} C_p\rho(\mathbf{V}\theta).\mathbf{n}dydz \equiv F_{GC} \quad (5)$$

(Wm^{-2}) at the GC entrance (α is the area of the cross section), since in the past it had been obtained for geostrophic advection either from very scant data [*Ripa*, 1997] or at a single cross section [*Mascarenhas et al.*, 2004]. The values of F_{GC} for each cross section sampled during this study are shown in the first two rows of Table 3, using both the LADCP velocity and the geostrophic velocity (the latter assuming no motion at 1500 m, for consistency with previous calculations (geostrophic velocity distributions are presented in auxiliary material).

[58] There is a good agreement between the geostrophic and the LADCP heat advection estimates of F_{GC} (Table 3), which suggests that the directly measured currents were mostly in geostrophic equilibrium. However, the values vary widely between sections, so much so that differences between sections can have either sign! This is reflected in the large standard deviation. The reason for this wide variability in F_{GC} is the real variability (in time and space) of the hydrodynamics and thermodynamics. As additional evidence that such variability is to be found in the GC at

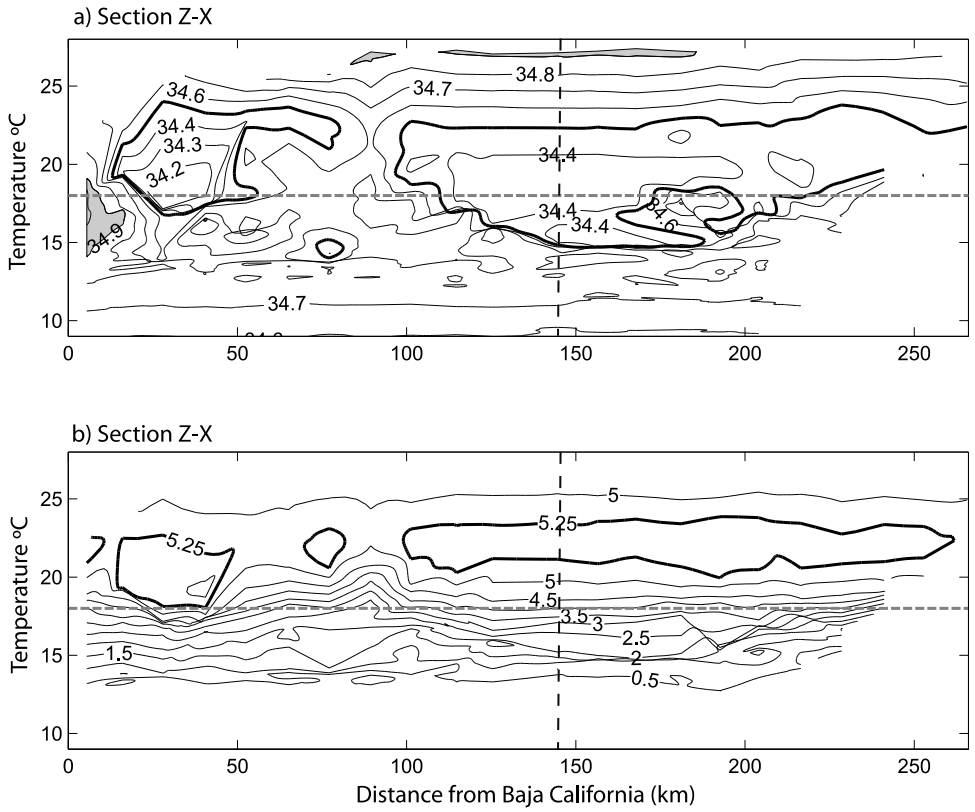

Figure 15. Distribution of (a) salinity and (b) dissolved oxygen (ml l^{-1}) on the θ distance "space," for joint sections Z and X. The GCW is marked in dark gray, and the 34.5 isohaline in dark black. The gray dotted line is the 18°C isotherm, which marks the boundary between the TSW and StSsW. The vertical dashed line is where sections Z and X join.

other times, the third row of Table 3 shows the geostrophic advection of heat calculated to 1500 m at three cross sections, made in 24–31 May 1998 [*Castro et al.*, 2000, 2006], similar to some of the ones presented here.

[59] The last column of Table 3 shows the average of the lateral heat fluxes from all the sections. Since it contains all the variability present during the period of observation, we believe that they represent the best estimate available of the lateral (advective) heat flux into the GC, albeit for 7–17 June 2004. The mean value 4.8×10^5 Wm^{-2} (equivalent to 121 TW when multiplied by the cross-sectional area) is larger than previous estimates for June: *Castro et al.* [1994] obtained 21 TW, *Ripa* [1997] estimated 59 TW, and *Mascarenhas et al.* [2004] estimated 27 TW. Our interpretation of this large value is that during the NAME-1 cruise we sampled a very intense advective event, triggered by a decaying mesoscale eddy.

4.4. Inflowing Currents

[60] The LADCP data show that at the time of the observation there were two inflows, one through section Z, which reached from the surface to beyond 1000 dbar, and another through section X, which was weak in the surface but fast at depth (50–500 m). The former was associated with the decaying anticyclonic eddy, and provided 6 of the 8 Sv entering the GC though section A; the inflow through section X provided the remaining 2 Sv and seems to have been associated with the Mexican Coastal Current, possibly strengthened by a CTW. These two inflows could be the reason for the double inflow lobes seen in the LADCP data ($\mathbf{V}_{24}$ in sections B and C in Figures 13a–13b, and at depth in Figure 10).

[61] The inflow of tropical water on the mainland side, and outflow of GCW on the peninsula side have been mentioned since the early works of *Roden and Groves* [1959] and up until *Castro et al.* [2006] but this is the first time that a three-dimensional time-variable description has been given, based on directly measured currents (LADCP and drifters) and supported by simultaneous satellite images.

[62] The conception of the inflowing current on the mainland shelf has changed in recent years. Previously it was suggested that it could be an extension of the poleward Costa Rica Coastal Current, which according to *Wyrtki* [1967] reached the Gulf entrance in summer. However, the recent description of the Eastern Tropical Pacific circulation by *Kessler* [2006] does not find a clear connection between the Costa Rica Coastal Current and the Mexican Coastal Current. Numerical models [*Beier et al.*, 2003; *Zamudio et al.*, 2007, 2008] and satellite altimetry [*Strub and James*, 2002] show that in the mean and for most of the year these two currents are disconnected. *Zamudio et al.* [2007] have numerically shown that the Mexican Coastal

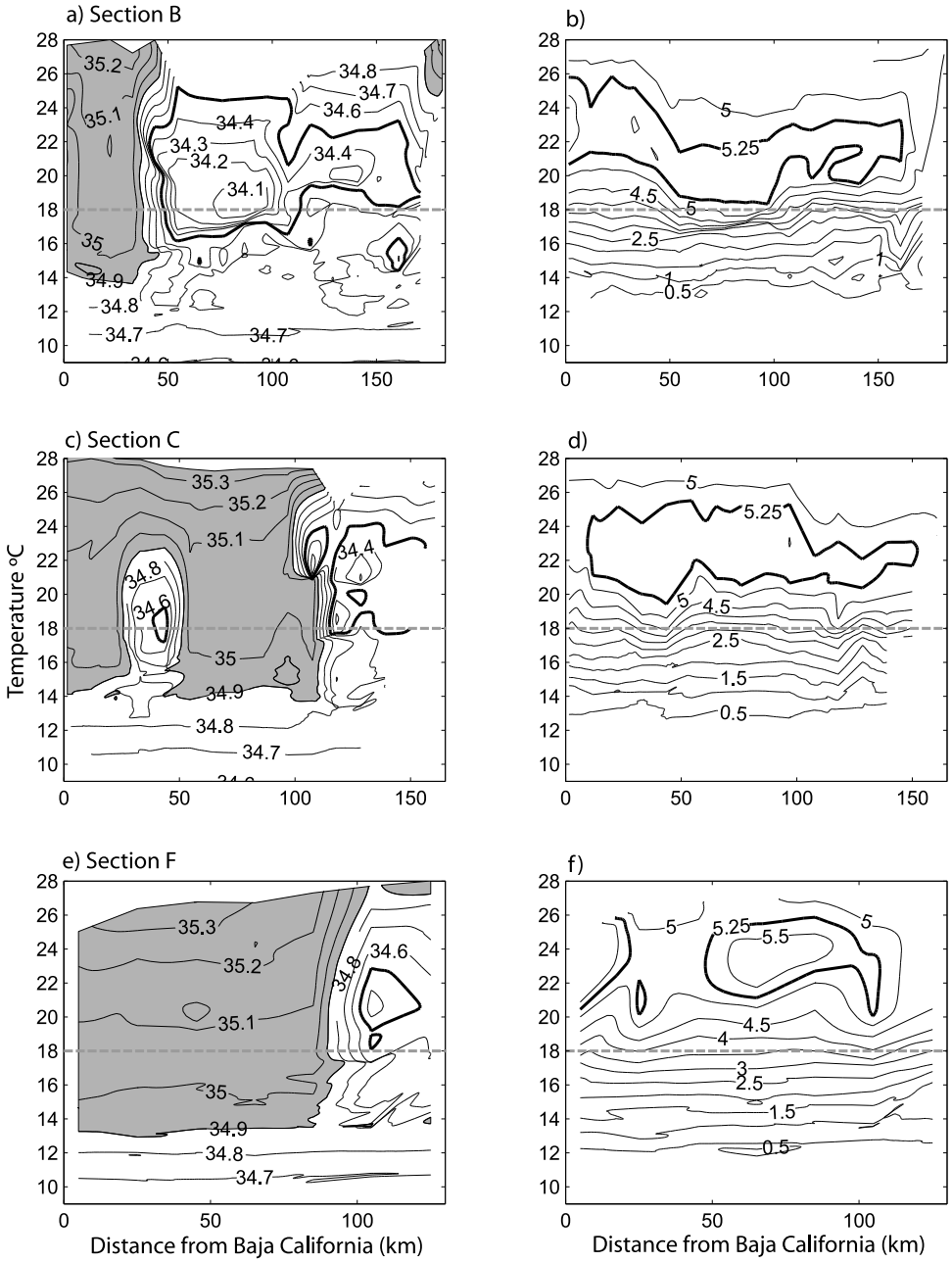

Figure 16. Distribution on the θ-distance "space," of (left) salinity and (right) dissolved oxygen (ml l^{-1}) for sections (a) B, (b) C, and (c) F. The GCW is marked in dark gray, and the 34.5 isohaline is marked in dark black. The gray dotted line is the 18°C isotherm, which marks the boundary between the TSW and StSsW.

Current is forced by the local wind stress curl in Sverdrup balance.

4.5. Water Masses

[63] While identifying the high-salinity water inside and on the western side of the Gulf as GCW is straightforward, care is needed for the remaining waters. Even for the GCW there are two distinct kinds: (1) that in the peninsula side in the inner sections, occupying from the surface to 100–150 dbar (Figures 8 and 9) which is seen flowing out of the GC as a narrow deep stream (Figures 10 and 11), and (2) the water occupying 0–40 dbar in the mainland shelf and in the crossing of sections Z and X (Figures 8, 9, and 13), and flowing into the Gulf. The former is Gulf of California Water, formed by winter convection in the Northern Gulf, as indicated by its low temperature (12–18°C). The latter is TSW that has been subjected to evaporation but its high temperature keeps it in the surface layer [*Castro et al.*, 2000; *Lavín and Marinone*, 2003; *Castro et al.*, 2006; *Lavín et al.*, 2006]. In the θ-S diagrams (Figure 6), the traces with GCW (in black) are characterized by salinity over 34.9 over a wide range of θ, while the traces with evaporated TSW have only a small fraction of

Table 4. Water Masses in the Entrance to the Gulf of California During the NAME-1 Cruise and the Range of Their Properties and Depth Distribution

Water Mass	Abbreviation	S	θ (°C)	γ_θ (kg m^{-3})	Depth (m)
Gulf of California Water	GCW	34.9–35.35	14–29.5	22.0–26.2	0–180
Evaporated Tropical Surface Water	eTSW	34.9–35.1	28–30	21.8–22.5	0–40
Tropical Surface Water	TSW	34.5–34.9	18–30	21.8–25	0–120
Shallow Salinity Minimum Water (California Current Water)	SSmW	34.1–34.5	16–25	23.2–25.6	10–110
Subtropical Subsurface Water*	StSsW	34.5–34.9	9–18	24.9–26.7	50–480
Pacific Intermediate Water	PIW	34.5–34.8	4–9	26.7–27.5	>400

the trace in the S $\geq$ 34.9 domain, and that at the highest temperatures.

[64] The surface cool anomaly had surface salinity between 34.8 and ~34.6, and since its temperature was above 18°C it would be identified as TSW, according to Table 1. However, Figure 8 suggests that the low salinity was part of a subsurface salinity minimum found throughout the entrance, approximately between 50 and 150 m, which had reached the surface because of the uplifted isotherms and isohalines.

[65] To get a better depiction of the distribution of the upper-layer water masses, the distributions of salinity on the isotherm versus across-Gulf distance "space" are shown in Figures 15 and 16 for some of the sections. Since the density field was dominated by temperature, these plots are very similar to the γ_θ versus distance plots (not shown). The distribution of dissolved oxygen (O_2) in the same space is also shown in Figures 15 and 16, as an aid in identifying water masses. In Figures 15 and 16, the GCW (S $\geq$ 34.9) is shown as dark shading and the isohaline of 34.5 psu as a thick contour.

[66] The salinity and dissolved oxygen distributions in this space for the combined Z + X section are shown in Figure 15. The StSsW was found between the lowest bound in the θ axis (9°C) and the 18°C isotherm (marked by a dashed horizontal gray line), and contained its distinctive salinity maximum (which in this section is 34.8 and was found between the 12 and 13°C isotherms, approximately). The only waters in the 9 to 18°C domain that were not StSsW are the intrusions of GCW close to the peninsula and the less-than-34.5 salinity intrusions.

[67] The TSW was found above the 18°C isotherm, and in Figure 15 it shared this space only with the less-than-34.5 salinity intrusions. In the inner cross sections, this space was also shared with GCW (section B, Figures 16a and 16b; section C, Figures 16c and 16d), which actually took most of the space in sections D, E, and F (section F, Figures 16e and 16f).

[68] As mentioned before, according to Table 1 most of the less-than-34.5 salinity intrusions would be classified as TSW because of their temperatures (17–24°C). However, the distribution of both S and O_2 suggest that this water had a different origin. Low-salinity intrusions like those shown here have been observed, most recently by *Castro et al.* [2000, 2006], who identified them as CCW. Previously, *Roden* [1971, 1972] called these salinity minimum intrusions (34.5–34.7) in the 50–100 m range the "shallow salinity minimum." Roden did not suggest an origin of the shallow salinity minimum, but *Warsh et al.* [1973] argued that it was a mixture of subsurface CCW and TSW (and called it Transition Water A), and found that it had an associated O_2 maximum. The salinity sections of *Roden* [1964, 1971, 1972] support the idea that CCW water is the main ingredient of the shallow salinity minimum. However, it is probably best to identify it as "Shallow Salinity Minimum Water" (SSmW) rather than as CCW as done hitherto [*Robles and Marinone*, 1987; *Bray*, 1988]. This shallow salinity minimum should not be confused with that found in the central-eastern tropical Pacific, which *Yuan and Talley* [1992] called Tropical Shallow Salinity Minimum. The study of the origin and time-space variability of this feature deserves further study, but it is beyond the scope of this article.

[69] In Figure 15a the shallow salinity minimum contained two distinct cores, one close to the peninsula (min. S ~ 34.2) and the other covering from the mainland to the offshore ends of sections Z and X (min. S ~ 34.4); the O_2 distributions (Figure 15b) supported this idea. The western core of SSmW was most extensive in section B (Figure 16a), where salinities below 34.1 were observed, but it stopped in section C (Figure 16b). By contrast, the eastern SSmW extends all the way to section F (Figure 16c), although very restricted to the mainland shelf. Quite clearly it was advected there by the strong currents, thus supporting the early suggestion of *Roden* [1964] and *Álvarez-Borrego and Schwartzlose* [1979] that traces of shallow salinity minima found further inside the GC was evidence of an inflowing current on the mainland side. The data presented here show that such is indeed the case.

[70] Finally, the properties of the water masses as observed in the NAME-1 cruise are summarized in Table 4, as an initial reconsideration of the definition of the water masses in the entrance to the GC, and more generally, in the subtropical-tropical transition zone of the eastern tropical Pacific. This is also a warning against blindly classifying water masses in this area using Table 1.

5. Conclusions

[71] The extensive observations made during the NAME-1 cruise in June 2004, both taken on board and from satellite-based sensors, provided the first three-dimensional time-variable description of the circulation and thermohaline structure in the entrance to the GC, at the phase of the seasonal cycle when the SST of the GC increases most rapidly.

[72] Of interest for the NAME, evidence was presented that the evolution of the surface distribution of SST in the zone was in great measure controlled by advection by inflowing coastal currents and by mesoscale features, although coastal upwelling off the western coasts also seems to contribute. It is therefore impossible to model the SST of the GC without including advection through the entrance. However, it was found that the advective heat flux into the Gulf of California presents very large variability in space

and time. For the NAME-1 cruise it was estimated that the lateral heat input was $4.8 \pm 3.0 \times 10^5$ Wm^{-2} as estimated with LADCP currents and $5.7 \pm 2.2 \times 10^5$ Wm^{-2} with geostrophic velocities.

[73] The main features of the circulation were as follows:

[74] 1. A stream entering from the south through section Z, covering from the surface to over 1000 m, which upon entering the Gulf flowed parallel to the mainland coast. This current appeared to be generated by mesoscale structures in the SST fronts south of the tip of the Baja California peninsula, in particular by an anticyclonic eddy that seemed to decay after interacting with the mainland coast.

[75] 2. A coastal current flowing from the SE parallel and off the mainland coast, probably identifiable as the Mexican Coastal Current. The combination of this current and that in the first feature caused very fast (up to 0.7 ms^{-1}) surface currents inside the GC.

[76] 3. An outgoing current carrying GCW close to the peninsula. It was mostly subsurface, 15–20 km wide, and reached to 500 m. It had a core of 0.2 to 0.4 ms^{-1} between 100 and 250 m.

[77] Overall, the data showed a dominance of advection over diffusion in controlling the thermohaline structure of the upper layers, as suggested by the sharp front between the water masses, and reflected also in the θ-S diagrams. Little recirculation was observed in the entrance (except perhaps in the innermost sections on the peninsula side), suggesting that the inflows penetrated deep into the Gulf, injecting TSW, SSmW, and StSsW.

[78] **Acknowledgments.** This is a product of project "The Role of Oceanic Processes on the Gulf of California SST Evolution during the North American Monsoon Experiment," which is part of the North American Monsoon Experiment (NOAA contract GC04–219, P.I. Michael Douglas). This work was also supported by CONACyT (Mexico) projects D41881-F (P.I., MFL) and C01–25343 (P.I., RC), by UABC projects (P-0324 and P-0352) and by CICESE. VMG held a CONACYT scholarship. MFL was at SIO-UCSD as recipient of a UCMEXUS-CONACYT sabbatical scholarship, hosted by P. Niiler, while working on this article. Thanks to Mayra Pazos and the Drifter Data Assembly Center (GDP/NOAA) for handling drifter data. Technical support by C. Cabrera, R. Camacho, J. García, and C. Flores. We thank the support of the skipper and crew of the B/O Francisco de Ulloa.

References

Álvarez-Borrego, S., and R. A. Schwartzlose (1979), Water masses of the Gulf of California, *Cienc. Mar.*, *6*(1), 43–63.

Álvarez-Sánchez, L. G., E. G. Stevenson, and B. Wyatt (1978), Circulación y masas de agua en la región de la boca del Golfo de California en la primavera de 1970, *Cienc. Mar.*, *5*(1), 57–69.

Amador-Buenrostro, A., A. Trasviña-Castro, A. Muhlia-Melo, and M. Argote-Espinoza (2003), Influence of EBES Seamount and Farallón Basin on coastal circulation in the Gulf of California, Mexico, *Geofis. Int.*, *42*, 407–418.

Beier, E. (1997), A numerical investigation of the annual variability in the Gulf of California, *J. Phys. Oceanogr.*, *27*(5), 615–632, doi:10.1175/1520-0485(1997)027<0615:ANIOTA>2.0.CO;2.

Beier, E., M. F. Lavín, J. Gómez, V. M. Godínez, and J. García (2003), La Corriente Costera Mexicana, in *GEOS, Reunión Anual 2003 de la Unión Geofísica Mexicana*, vol. 23, p. 152, Puerto Vallarta, Mexico.

Beron-Vera, F. J., and P. Ripa (2000), Three-dimensional aspects of the seasonal heat balance in the Gulf of California, *J. Geophys. Res.*, *105*(C5), 11,441–11,457, doi:10.1029/2000JC900038.

Beron-Vera, F. J., and P. Ripa (2002), Seasonal salinity balance in the Gulf of California, *J. Geophys. Res.*, *107*(C8), 3100, doi:10.1029/2000JC000769.

Bordoni, S., P. E. Ciesielski, R. H. Johnson, B. D. McNoldy, and B. Stevens (2004), The low-level circulation of the North American Monsoon as revealed by QuikSCAT, *Geophys. Res. Lett.*, *31*, L10109, doi:10.1029/2004GL020009.

Bray, N. (1988), Water mass formation in the Gulf of California, *J. Geophys. Res.*, *93*(C8), 9223–9240, doi:10.1029/JC093iC08p09223.

Cabrera, C. E., M. F. Lavín, and E. Beier (2006), Monitoreo satelital de la superficie del océano y su aplicación en cruceros oceanográficos, *Rep. 50103*, 99 pp., Dep. de Oceanogr. Fis., CICESE, Ensenada, Mexico. (Available at http://oceanografia.cicese.mx/index.php?file=reportestec2006)

Castro, R., M. F. Lavín, and P. Ripa (1994), Seasonal heat balance in the Gulf of California, *J. Geophys. Res.*, *99*, 3249–3261, doi:10.1029/93JC02861.

Castro, R., A. Mascarenhas Jr., R. Durazo, and C. A. Collins (2000), Seasonal variation of the temperature and salinity at the entrance to the Gulf of California, México, *Cienc. Mar.*, *26*(4), 561–583.

Castro, R., R. Durazo, A. Mascarenhas Jr., C. A. Collins, and A. Trasvina (2006), Thermohaline variability and geostrophic circulation in the southern portion of the Gulf of California, *Deep Sea Res., Part I*, *53*(1), 188–200, doi:10.1016/j.dsr.2005.09.010.

Collins, C., N. Garfield, A. Mascarenhas Jr., M. Spearman, and T. Rago (1997), Ocean currents across the entrance to the Gulf of California, *J. Geophys. Res.*, *102*(C9), 20,927–20,936, doi:10.1029/97JC01302.

Emilsson, I., and M. A. Alatorre (1997), Evidencias de un giro ciclónico de mesoescala en la parte sur del Golfo de California, in *Contribuciones de la Oceanografía Física en México*, *Monogr. 3*, edited by M. F. Lavín, pp. 173–182, Unión Geofis. Mex., Mexico City.

Federov, K. N., and A. J. Ginsburg (1986), "Mushroom-like currents" (vortex dipoles) in the ocean and laboratory thank, *Ann. Geophys.*, *4*, 507–516.

Fernández-Barajas, M. E., M. A. Monreal, and A. Molina-Cruz (1994), Thermohaline structure and geostrophic flow in the Gulf of California, during 1992, *Cienc. Mar.*, *20*(2), 267–286.

Fiedler, P. C., and L. D. Talley (2006), Hydrography of the eastern tropical Pacific: A review, *Prog. Oceanogr.*, *69*(2–4), 143–180, doi:10.1016/j.pocean.2006.03.008.

Figueroa, M., G. Marinone, and M. F. Lavín (2003), Geostrophic gyres in the southern Gulf of California, in *Nonlinear Processes in Geophysical Fluid Dynamics*, edited by O. U. Velasco Fuentes, J. Sheinbaum, and J. Ochoa, pp. 237–255, Kluwer Acad., Dordrecht, Netherlands.

Filonov, A. E., and M. F. Lavín (2003), Internal tides in the Northern Gulf of California, *J. Geophys. Res.*, *108*(C5), 3151, doi:10.1029/2002JC001460.

Flament, P., L. Armi, and L. Washburn (1985), The evolving structure of an upwelling filament, *J. Geophys. Res.*, *90*(C6), 11,765–11,778, doi:10.1029/JC090iC06p11765.

Godínez, V. M., R. Castro, M. F. Lavín, and E. Beier (2006), Hydrography of the southern Gulf of California during the North American Monsoon Experiment: Campaign NAME-01, June 5–18, 2004, *Rep. 37259*, 199 pp., Dep. Oceanogr. Fis., CICESE, Ensenada, Mexico. (Available at http://oceanografia.cicese.mx/index.php?file=reportestec2006)

Griffiths, R. C. (1968), Physical, chemical, and biological oceanography of the entrance to the Gulf of California, spring of 1960, Bur. of Comm. Fish., U.S. Dept. of the Int., Washington, D. C.

Hansen, D., and P. M. Poulain (1996), Quality control and interpolations of WOCE-TOGA drifter data, *J. Atmos. Oceanic Technol.*, *13*, 900–909, doi:10.1175/1520-0426(1996)013<0900:QCAIOW>2.0.CO;2.

Higgins, R. W., Y. Chen, and A. V. Douglas (1999), Interannual variability of the North American warm season precipitation regime, *J. Clim.*, *12*(3), 653–680, doi:10.1175/1520-0442(1999)012<0653:IVOTNA>2.0.CO;2.

Higgins, W., and D. Gochis (2007), Synthesis of results from the North American Monsoon Experiment (NAME) process study, *J. Clim.*, *20*(9), 1601–1607, doi:10.1175/JCLI4081.1.

Kessler, W. S. (2006), The circulation of the eastern tropical Pacific: A review, *Prog. Oceanogr.*, *69*(2–4), 181–217, doi:10.1016/j.pocean.2006.03.009.

Kosro, P. M., and A. Huyer (1986), CTD and velocity surveys of seaward jets off northern California, July 1981 and 1982, *J. Geophys. Res.*, *91*(C6), 7680–7690, doi:10.1029/JC091iC06p07680.

Lavín, M. F., and S. G. Marinone (2003), An overview of the physical oceanography of the Gulf of California, in *Nonlinear Processes in Geophysical Fluid Dynamics*, edited by O.U. Velasco Fuentes, J. Sheinbaum, and J. Ochoa, pp. 173–204, Kluwer Acad., Dordrecht, Netherlands.

Lavín, M. F., E. Beier, J. Gómez-Valdés, V. M. Godínez, and J. García (2006), On the summer poleward coastal current off SW México, *Geophys. Res. Lett.*, *33*, L02601, doi:10.1029/2005GL024686.

Mascarenhas, A. S., R. Castro, C. A. Collins, and R. Durazo (2004), Seasonal variation of geostrophic velocity and heat flux at the entrance to the Gulf of California, Mexico, *J. Geophys. Res.*, *109*, C07008, doi:10.1029/2003jc002124.

Mitchell, D. L., D. Ivanova, R. Rabin, T. J. Brown, and K. Redmond (2002), Gulf of California Sea Surface Temperatures and the North American Monsoon: Mechanistic Implications from Observations, *J. Clim.*, *15*(17), 2261–2281, doi:10.1175/1520-0442(2002)015<2261:GOCSST>2.0.CO;2.

Navarro-Olache, L. F., M. F. Lavin, L. G. Alvarez-Sanchez, and A. Zirino (2004), Internal structure of SST features in the central Gulf of California, *Deep Sea Res., Part II*, *51*(6–9), 673–687.

Pegau, W. S., E. Boss, and A. Martinez (2002), Ocean color observations of eddies during the summer in the Gulf of California, *Geophys. Res. Lett.*, *29*(9), 1295, doi:10.1029/2001GL014076.

Relvas, P., and E. D. Barton (2002), Mesoscale patterns in the Cape Sao Vicente (Iberian Peninsula) upwelling region, *J. Geophys. Res.*, *107*(C10), 3164, doi:10.1029/2000JC000456.

Ripa, P. (1997), Toward a physical explanation of the seasonal dynamics and thermodynamics of the Gulf of California, *J. Phys. Oceanogr.*, *27*(5), 597–614, doi:10.1175/1520-0485(1997)027<0597:TAPEOT>2.0.CO;2.

Robles, J. M., and S. G. Marinone (1987), Seasonal and interannual thermohaline variability in the Guaymas Basin of the Gulf of California, *Cont. Shelf Res.*, *7*(7), 715–733, doi:10.1016/0278-4343(87)90013-6.

Roden, G. I. (1964), Oceanographic aspects of Gulf of California, Marine geology of the Gulf of California: A symposium, *Am. Assoc. Petrol. Geol. Mem.*, *3*, 30–58.

Roden, G. I. (1971), Aspects of the transition zone in the Northeastern Pacific, *J. Geophys. Res.*, *76*(15), 3462–3475, doi:10.1029/JC076i015p03462.

Roden, G. I. (1972), Thermohaline structure and baroclinic flow across the Gulf of California entrance and in the Revilla Gigedo Islands region, *J. Phys. Oceanogr.*, *2*(2), 177–183, doi:10.1175/1520-0485(1972)002<0177:TSABFA>2.0.CO;2.

Roden, G. I., and G. W. Groves (1959), Recent oceanographic investigations in the Gulf of California, *J. Mar. Res.*, *18*, 10–35.

Send, U., R. C. Beardsley, and C. D. Winant (1987), Relaxation from upwelling in the Coastal Ocean Dynamics Experiment, *J. Geophys. Res.*, *92*, 1683–1698, doi:10.1029/JC092iC02p01683.

Smith, S. D. (1988), Coefficients for sea surface wind stress, heat flux, and wind profiles as a function of wind speed and temperature, *J. Geophys. Res.*, *93*(C12), 15,467–15,472, doi:10.1029/JC093iC12p15467.

Soto-Mardones, L., S. G. Marinone, and A. Parés-Sierra (1999), Time and spatial variability of sea surface temperature in the Gulf of California, *Cienc. Mar.*, *25*, 1–30.

Strub, P. T., and C. James (2002), Altimeter-derived surface circulation in the large-scale NE Pacific Gyres.: Part 1. Seasonal variability, *Prog. Oceanogr.*, *53*(2–4), 163–183, doi:10.1016/S0079-6611(02)00029-0.

UNESCO (1991), *Processing of Oceanographic Station Data*, *Tech. Pap. Mar. Sci.*, 138 pp., Paris.

Visbeck, M. (2002), Deep velocity profiling using lowered acoustic doppler current profilers: Bottom track and inverse solutions, *J. Atmos. Oceanic Technol.*, *19*(5), 794–807, doi:10.1175/1520-0426(2002)019<0794:DVPULA>2.0.CO;2.

Warsh, C., and K. Warsh (1971), Water exchange at the mouth of the Gulf of California, *J. Geophys. Res.*, *76*(33), 8098–8106, doi:10.1029/JC076i033p08098.

Warsh, C. E., K. L. Warsh, and R. C. Staley (1973), Nutrients and water masses at the mouth of the Gulf of California, *Deep Sea Res. Oceanogr. Abstr.*, *20*(6), 561–570, doi:10.1016/0011-7471(73)90080-6.

Wyrtki, K. (1967), Circulation and water masses of the eastern tropical Pacific Ocean, *Int. J. Oceanogr. Limnol.*, *1*, 117–147.

Yuan, X., and L. D. Talley (1992), Shallow salinity minima in the North Pacific, *J. Phys. Oceanogr.*, *22*(11), 1302–1316, doi:10.1175/1520-0485(1992)022<1302:SSMITN>2.0.CO;2.

Zamudio, L., H. E. Hurlburt, E. J. Metzger, and C. E. Tilburg (2007), Tropical wave-induced oceanic eddies at Cabo Corrientes and the Maria Islands, Mexico, *J. Geophys. Res.*, *112*, C05048, doi:10.1029/2006JC004018.

Zamudio, L., P. Hogan, and E. J. Metzger (2008), Summer generation of the Southern Gulf of California eddy train, *J. Geophys. Res.*, *113*, C06020, doi:10.1029/2007JC004467.

Zuidema, P., C. Fairall, L. M. Hartten, J. E. Hare, and D. Wolfe (2007), On air-sea interaction at the mouth of the Gulf of California, *J. Clim.*, *20*(9), 1649–1661, doi:10.1175/JCLI4089.1.

A. Amador, V. M. Godínez, and M. F. Lavín, Departamento de Oceanografía Física, CICESE, Ensenada, 22860, Mexico. (mlavin@cicese.mx)

E. Beier, Estación La Paz, CICESE, Miraflores 334, Fraccionamiento Bellavista, La Paz, 23050, Mexico.

R. Castro, Facultad de Ciencias Marinas, Universidad Autónoma de Baja California, Apartado Postal 453, Ensenada, 22800, Mexico.

P. Guest, Department of Meteorology, Naval Postgraduate School, Monterey, CA 93943, USA.